Icarus 390 (2023) 115320

Contents lists available at ScienceDirect

Icarus

journal homepage: www.elsevier.com/locate/icarus

A new prospect to analyse the spectral properties of v-type asteroids

M. Angrisani *, E. Palomba, A. Longobardo, A. Raponi, F. Dirri, C. Gisellu

INAF-IAPS Rome, Via Fosso del Cavaliere,100 Rome, Italy

ARTICLE INFO

Keywords:
Spectroscopy
Asteroids, surfaces
Regoliths
Asteroids
Composition

ABSTRACT

Among main belt asteroids, some have a spectrum similar to Vesta so they are taxonomically classified as V-type asteroids. Probably they were removed from Vesta and migrated to their current positions via some still unknown dynamical mechanisms. Several issues on the relationship between V-type asteroids, Howardite-Eucrite-Diogenite (HED) meteorites and Vesta are still unresolved. Although some of them can be directly linked to (4) Vesta, forming its dynamical family, others do not appear to have a clear dynamical link, thus suggesting the existence of other basaltic parent bodies. In this work we present a new approach of analysis to investigate 76 VNIR V-type asteroids spectra downloaded from PDS. The composition of the regolith and particle size of V-type asteroid have been investigated with a combination of spectroscopic analysis and Hapke radiative transfer model. Retrieved particle sizes are very small, with a mean value of 20 μm.

Therefore, we look for statistically significant differences among the modal mineralogy of V-type asteroids belonging to different dynamical subclasses. It seems there is a possible chronologic link between impact events on Vesta and the V-type families. The most ancient V-type family, e.g. Low-I asteroids, seems to have a eucritic composition compatible with an ejection of the outermost layer of Vesta. The Fugitive V-type were probably ejected in an older cratering event that produced the Veneneia basin while the Vestoids family, whose dynamical parameters are still more similar to Vesta and which seems to be the youngest family among them, could be associated to Rheasilvia basin. The last two families seem to have a diogenitic composition compatible with that of the south of Vesta, where the two huge craters are located.

Spartacus asteroid is also analysed and it was found to have a modal mineralogy consistent with the presence of olivine as noted before (Moskovitz et al.,2010; Burbine et al., 2001).

1. Introduction

(4) Vesta is the second most massive body in the main asteroid belt. The Dawn mission has provided new insight about Vesta (e.g., De Sanctis et al., 2012, 2013; Jaumann et al., 2014; Williams et al., 2014) and new evidence concerning the link between Vesta and Howardite-Eucrite-Diogenite (HED) meteorites (McSween et al., 2013). VIR spectra of Vesta's surface show ubiquitous absorption bands centred at approximately 0.9 and 1.9 μm, confirming the presence of iron-bearing low-calcium pyroxenes, and are very similar to HED (McCord et al., 1970; Ammannito et al., 2013; McSween et al., 2013). Howardite – eucrite – diogenite (HED) meteorites are igneous rocks or breccias composed of fragmented igneous rocks. Eucrites are dominated by pyroxenes and plagioclase, with lower amounts of metal, troilite, chromite, ilmenite, and silica. Most eucrites are brecciated (McSween et al., 2011; Mittlefehldt et al., 2015), while the majority of diogenites are coarse-grained ultramafic rocks dominated for the most part by orthopyroxene (Mittlefehldt et al., 2015). The olivine abundance ranges between 0 and 33 vol%, being most common in diogenites (Mittlefehldt et al., 2015). Due to the brecciation of diogenites, significant amounts of plagioclase and diopside can be attributed to the incorporation of eucrite fragments (McSween et al., 2011). Instead, Howardites are mostly composed of diogenitic and eucritic debris (Mittlefehldt et al., 2015). Furthermore, HED have generally common minor phases as Troilite (≤3 vol%) and metal (≤1 vol%) in the form of opaque grains (Mittlefehldt et al., 2015).

The discovery of new basaltic objects far away from Vesta but taxonomically classified as V-type a (DeMeo et al., 2009) has opened new questions about the origins of the many different V-type asteroids. Some of them can be traced back to Vesta through dynamical pathways (Carruba et al., 2007, Nesvorny et al., 2008). Other small basaltic asteroids in the outer and intermediate main belts (Lazzaro et al., 2000; Hammergren et al., 2006; Moskovitz et al., 2008; Roig et al., 2008; Duffard and Roig, 2009), as well as in the inner belt, but far away from

* Corresponding author.
E-mail address: marianna.angrisani@inaf.it (M. Angrisani).

https://doi.org/10.1016/j.icarus.2022.115320
Received 19 April 2022; Received in revised form 5 October 2022; Accepted 18 October 2022
Available online 23 October 2022

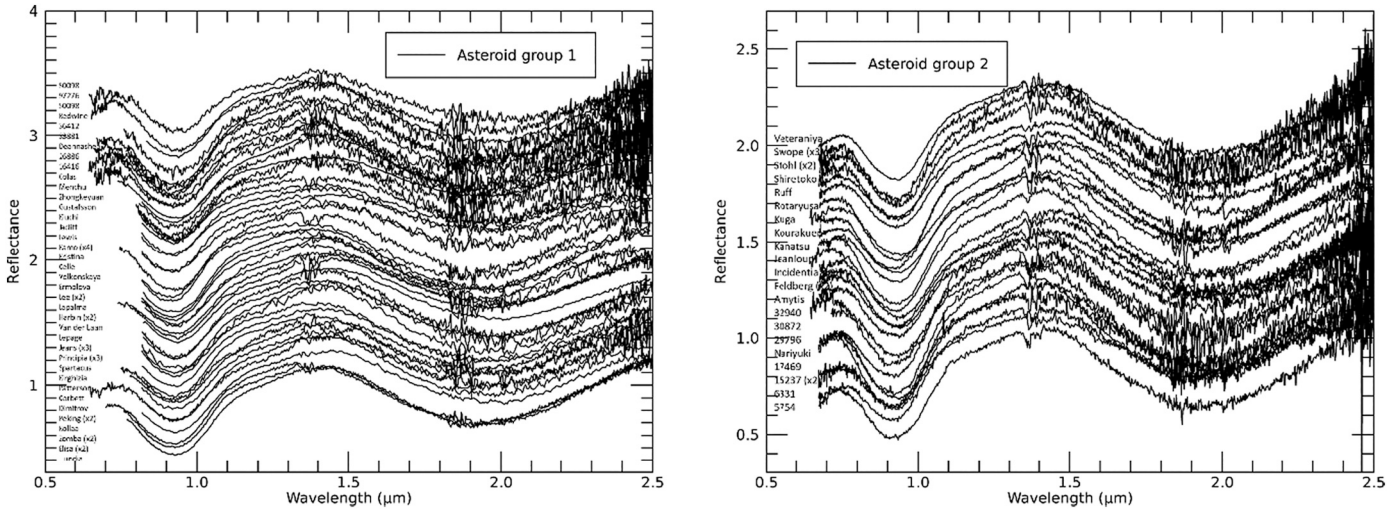

Fig. 1. VNIR spectra for the V-type asteroids of (left) group 1 (e.g. spectra normalized at 1.215 μm) and (right) group 2 (e.g. spectra normalized at 1.5 μm). All spectra are shifted on the vertical axes for clarity.

the dynamical limits of the Vesta family (e.g. Duffard et al., 2004), could confirm that several differentiated parent bodies must have formed. Furthermore, Vesta underwent two huge impact events (Marchi et al., 2012). One Ga ago, a massive collision was responsible for the Rheasilvia crater, while Veneneia crater (which underlies Rheasilvia basin) is believed to be older ($\geq$ 1 Ga). Probably, there is a chronologic link between impact events on Vesta and the V-type asteroids that are thought to have eventually supplied the HEDs to nearby escape hatches from the Main Belt. Indeed, the spectral diversity observed between V-type is supposed to be due to the distinct composition present on these asteroids, which in turn reflects the compositional differentiation observed on Vesta surface (De Sanctis et al., 2011; Duffard et al., 2004).

De facto, on Vesta there is a locally well-mixed superficial regolith with fine particle size, as suggested by spectroscopical and thermophysical analysis (De Sanctis et al., 2013; Palomba et al., 2014, 2019; Capria et al., 2014). Dawn confirmed that Vesta has a composition spanning from the eucritic to the diogenitic and found a strong dichotomy between the southern and northern hemispheres (De Sanctis et al., 2012). The VIR spectrometer showed that there are considerable regional and local albedo and compositional variations across the asteroid, and that diogenitic components are concentrated mainly in the southern region, particularly matching the Rheasilvia impact basin (De Sanctis et al., 2012). Furthermore, surface brightness is not uniform, and bright and dark material units are observed, where a dark region is defined in Palomba et al. (2014) as a region with a reflectance lower than a certain threshold i.e., a region darker than the surroundings that allows to identify the presence of a darkening end-member even in brighter regions. The dark units of Vesta show the same spectral features of the average Vesta spectrum, weakened due to the presence of darkening agents. Furthermore, these areas show a positive correlation between low albedo and the OH band centred at 2.8 μm, confirming the hypothesis that the darkening agents are carbonaceous chondrites, probably delivered by low-velocity impacts of primitive asteroids (Palomba et al., 2014; McCord et al., 2012).

In this work, we considered four dynamical families of V-type as follows:

(i) Vestoid: a V-type member of the Vesta dynamical family, as defined by Nesvorny using the Hierarchical Clustering Method (HCM).

(ii) Fugitive: following the definition of Nesvorny et al. (2008), is a V-type asteroid with a $<$ 2.3 au and comparable e and i with the Vesta family.

(iii) Low-I: according to Nesvorny et al. (2008) it is a V-type asteroid having $i < 6^{\circ}$ and 2.3 $<$ a $<$ 2.5 au.

(iv) IOs (Inner Others): the remaining V-type asteroids in the inner main belt.

Then, possible scenarios on the formation of V-type asteroids family are suggested (Moskovitz et al., 2010; Ieva et al., 2016). V-type asteroids that do not appear spectroscopically different from Vesta could represent an older population of Vesta family objects if they were removed from Vesta in its early phases of formation and were scattered to their current location due to the sweeping of mean motion resonances, or these objects were removed at the epoch of the Vesta family formation and migrated to their current position via some still unknown dynamical mechanisms. Also, there could be V-types from bodies different from Vesta even if they are (within error bars) spectrally identical to Vesta and other early asteroids could have gone through the same thermal evolution as Vesta.

In this work, we aim to infer the regolith particle size and composition of 76 V-type asteroids observed from Earth (Moskovitz et al., 2010; Hardersen et al., 2014, 2015, 2018) using a spectroscopic analysis and the Hapke Radiative Transfer Model (hereafter also called Hapke RTM). Then, we investigate the connection between V-type asteroids family and Vesta from the compositional and dynamical properties point of view.

The spectral data employed are shown in Section 2 while the spectral parameters suitable for the analysis and the used tools are described in Section 3. In Section 4, we present the results on HED and V-type asteroids applying the tools described in the previous section, whereas in Section 5 we discuss the modal composition of some asteroids, the statistical analysis of the V-type family and their correlation with Vesta. Finally, conclusions are given in Section 6.

2. Data

V-type asteroid spectra were obtained from SpeX ground based observations and are available on the Planetary Data System (PDS). The SpeX instrument is one of the most significant developments in ground-based characterization of small bodies at the NASA Infrared Telescope Facility (IRTF) in Mauna Kea, Hawaii. Calibration and reduction of data employed the Spextool package, therefore in Moskovitz et al. (2010)[1] (hereafter named as group 1) all spectra were scaled by fitting a polynomial over the region centred on the J-band (1.215 μm), and then

[1] [Bus, S. J., Ed. (202). IRTF Near -IR Spectroscopy of Asteroids V1.0. urn: nasa:pds:gbo.ast.irtf -spex -collection.spectra::1.0. NASA Planetary Data System; https://doi.org/10.26033/ct3r-eh13]

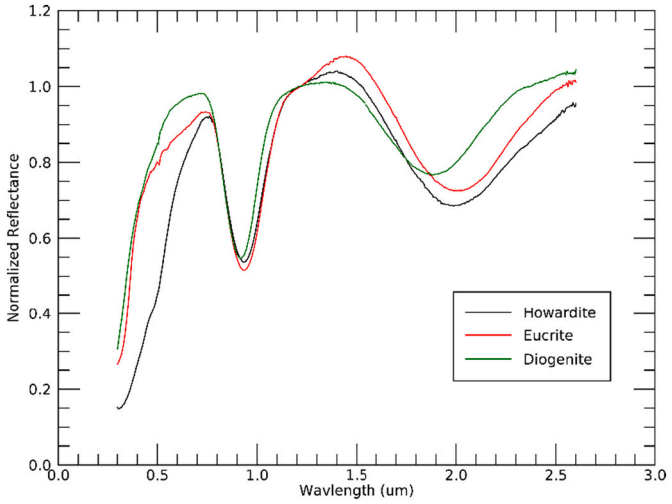

Fig. 2. Example of VNIR spectra for the Howardite, Eucrite and Diogenite meteorites normalized at 1.215 μm. The spectra are dominated by two pyroxene absorption bands respectively centred at about 0.9 μm and 1.9 μm. Both bands shift regularly to longer wavelengths with increasing Fe and/or increasing Ca content (Cloutis and Gaffey, 1991; Klima et al., 2008).

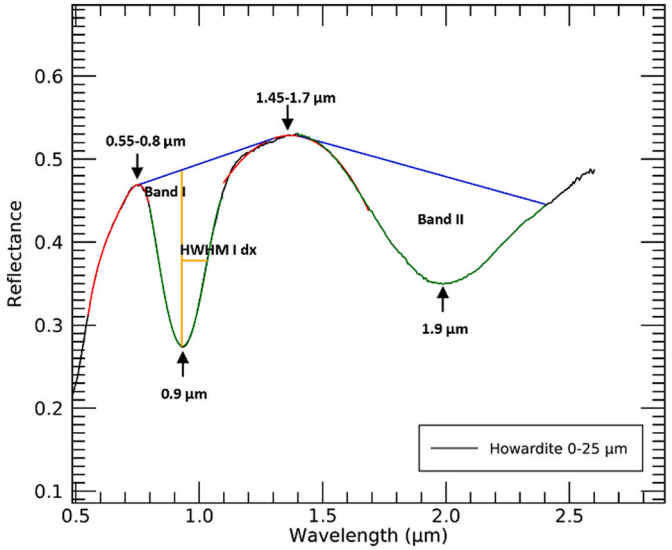

Fig. 3. Typical spectrum of a Howardite (with the particle size range of 0 -25 μm) showing the spectral features chosen as being diagnostic.

normalizing the fitted value at 1.215 μm to 1.00 (Fig. 1 left side), while in Hardersen et al. (2014, s2015, 2018) data[2] (hereafter named group 2) were normalized at 1.5 μm (Fig. 1 right side).

Since V-type asteroids are supposed to be the parent objects of HED (Fig. 2) (McSween et al., 2013; De Sanctis et al., 2013), in this work we compare the results obtained from V-type asteroids with HED meteorites (with known size intervals), as used in Palomba et al., 2014, whose spectra are available in the NASA Reflectance Experiment LABoratory (RELAB) database at Brown University.

[2] [Hardersen, P.S., Hardersen IRTF Asteroid NIR Reflectance Spectra V1.0. EAR -A -I0046 -3 -HARDERSENSPEC -V1.0. NASA Planetary Data System, 2016."].

3. Tools:

3.1. Spectroscopic analysis

VNIR Spectra of V-type asteroids, HED and Vesta are dominated by two pyroxene absorption bands, commonly referred to as Band I and Band II and respectively centred at about 0.9 μm and 1.9 μm.

Band I and Band II of pyroxenes shift regularly to longer wavelengths with increasing Fe and/or increasing Ca content (Cloutis and Gaffey, 1991; Klima et al., 2008).

De facto pyroxenes have two distinctive octahedral sites, M1 and M2. The M2 site is larger and more distorted than the M1 site and thus contains large cations such as Ca^{2+}. When Fe^{2+} and Mg are present, Fe^{2+} prefers the M2 site over the M1 site because Fe^{2+} is slightly larger. However, this preference is not absolute, and the amount of Fe^{2+} partitioned into the M1 and M2 sites depends on the bulk composition of the pyroxene, temperature and pressure of formation, cooling rate, and subsequent metamorphism.

In our case, in order to study the spectral properties and to understand the mineral composition and possibly the physical characteristics of the asteroid regolith (i.e., effective particle size), we introduce spectral parameters such as the band centre (BC), the band depth (BD) and Half Width Half Maximum (HWHM) (Fig. 3). These spectral parameters have been found to be useful for extracting helpful information (Palomba et al., 2014; Burbine et al., 2009).

Band centre is defined as the band minimum after the spectral continuum removal, while band depth is:

$$BD = 1 - Rb/Rc$$

Where Rb and Rc are the reflectance of the band and the spectral continuum at the band centre (Cloutis and Gaffey, 1991).

However, to better characterize the spectral parameters of each band, we need the spectrum to include both visible and near IR spectral intervals. Typically, this is not a problem when considering HED spectra that are taken by using laboratory spectrometers. The case of ground -based asteroids spectral data is different, the shorter wavelength is often located at ≈0.8 μm and therefore the spectra do not cover the entire Band I spectra, making the calculation of the corresponding band parameters difficult. Nevertheless, from HED laboratory studies, Cloutis and Gaffey (1991) suggests to add 7 nm to Band I minimum. So, in this work, Band centre I (0.9 μm) is defined 7 nm long -ward of band minima (Cloutis and Gaffey, 1991), whereas Band centre II is the band minimum after the spectral continuum removal.

Another spectral parameter that is useful to characterize the studied minerals is the Half -Width Half Maximum (HWHM), defined as the distance between the wavelength corresponding to the half of shoulder reflectance and the band minimum. We define HWHM I dx (dextrum, i.e., right) the distance between the wavelength corresponding to the half of long wavelength shoulder of band I and the band I minimum wavelength (Fig. 3).

Following an approach similar to Palomba et al. (2014) and Longobardo et al. (2014), fourth -order polynomial fits have been used to fit the Band I shoulder (between 0.55 and 0.80 μm, if it is possible, and between 1.10 and 1.69 μm respectively) and the Band I and Band II reflectance troughs (between 0.80 and 1.10 μm and between 1.81 and 2.07 μm respectively). Band I continuum is defined as the straight line starting from the ≈0.7 μm maximum and tangent to the spectral curve. When VIS wavelength data are lacking, the straight line starts from ≈0.8 μm and is tangent to the spectral curve. Band II continuum is the straight line from the maximum between 1.10 and 1.69–2.40 μm. Typically, the 2.40 μm cut is justified by the possible presence of a water band in laboratory samples, which could affect the retrieval of the spectral parameters relative to Band II (Palomba et al., 2014; Longobardo et al., 2014). In addition, in case of asteroids spectra, especially for those quite noisy, it is difficult to determine the exact band II position due to low S/N, therefore spectra were previously smoothed.

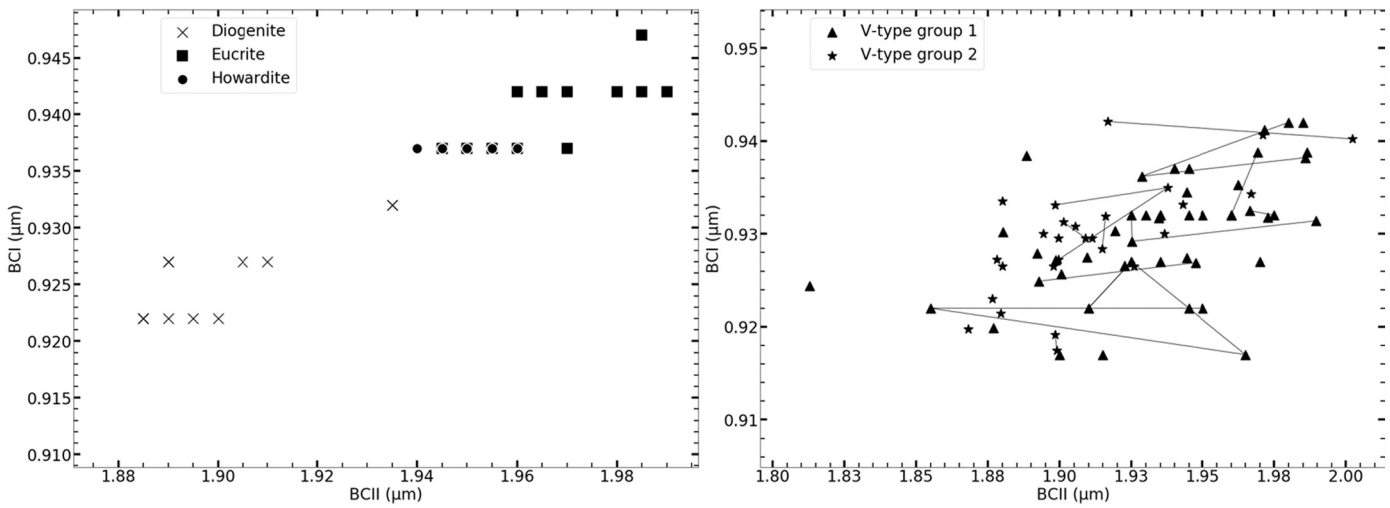

Fig. 4. Band I Centre versus Band II Centre scatterplot of HED (left) and V-type asteroids (right) normalized at 1.215 μm (group 1 - triangles) and normalized at 1.5 μm (group 2 -stars). This scatterplot helps to infer the composition of HED and of V-type asteroids. Band centers located at shorter wavelengths correspond to diogenitc composition, whereas longer wavelengths correspond to eucritic composition. Asteroidal multiple observations are linked by a line.

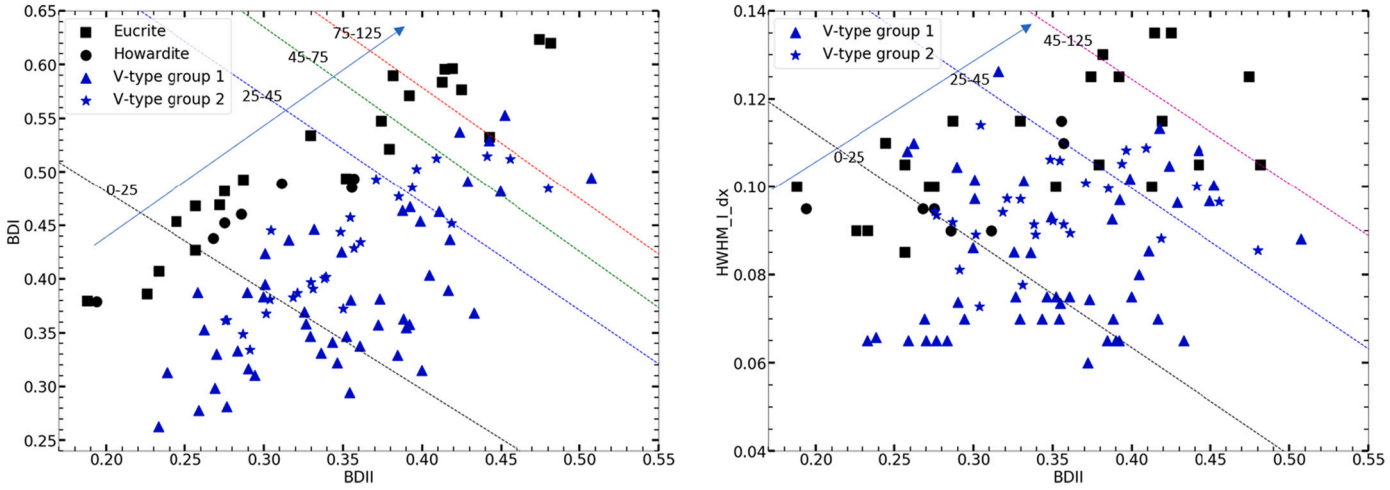

Fig. 5. BDI versus BDII scatterplot (left) and HWHM I dx versus BDII (right) on Eucrite (squares), Howardite(circles) and V- normalized at 1.215 μm (group 1 - triangles) and normalized at 1.5 μm (group 2 -starsThe dotted lines stand for the median of cluster of HED of particle size of 0 -25, 25 -45, 45 -75, 75 -125 (or 45 -125) μm. The arrow shows the direction of the increasing particle size.

To estimate the errors on spectral parameters introduced by the method applied, we followed Galiano et al. (2018) approach. In other words, we assumed the uncertainty associated to the spectral parameters as the variation between the spectral parameters on a spectrum without fit and a spectrum with fit, since the fitting procedure can introduce errors in the calculated parameters. When no variation arise, the spectral sampling is assumed as error. This method is a conservative approach that should best approximate the errors in spectral parameters determinations.

3.2. Radiative transfer model

Radiative Transfer Models (RTM) are widely used tools for compositional analyses of planetary bodies. Models of radiative transfer on atmosphereless bodies generally can provide insight into particle sizes, mineral compositions, and mineral abundances (Lucey, 1998.

The particular version of RTM is the Hapke model that is best presented in Hapke et al. (1981, 2012) as the bidirectional reflectance. This is defined as the ratio of the radiant power received per unit area per unit solid angle by a detector viewing a surface from an angle of emergence $=cos^{-1}\mu$, the surface being illuminated from an angle of incident $i = cos^{-1}\mu_0$, by collimated light, to the radiant power per unit area from the source (Hapke et al., 1981, 2012). The bidirectional reflectance equation is:

$$r(\mu_0,\mu,g) = \frac{\omega}{4\pi}\frac{\mu_0}{\mu_0+\mu}\{[1+B(g)]P(g)+H(\mu_0)H(\mu)-1\}$$

where g is the phase angle, ω is the single scattering albedo, P(g) is the single particle phase function, B(g) is the back scatter function, $H(\mu)$ and $H(\mu_0)$ are Chandrasekhar's functions.

Averaging, the total single scattering albedo is defined as following:

$$\omega = \frac{\sum_j \frac{M_j}{\rho_j d_j}\omega_j}{\sum_j \frac{M_j}{\rho_j d_j}}$$

Where M_j is the mass fraction of a mineral, ρ_j and d_j are average density and dimension of the particles of the j -th mineral. Phase function is given:

$$p(g) = 1 + bcosg + c\left[1.5cos^2 g - 0.5\right]$$

Table 1
Particle size range of Group 1 selected from Fig. 5. Minimum and maximum value are defined by the two closest lines, (showing the median value of cluster of HED with a defined particle size range) to the position of asteroid in scatterplot (Fig. 5).

	BDI versus BDII		HWHM versus BDII	
Name	Min (μm)	Max (μm)	Min (μm)	Max (μm)
809 Lundia	35	100	35	100
956 Elisa (1)	35	100	12.5	35
956 Elisa (2)	35	100	35	100
1468 Zomba (1)	0	12.5	0	12.5
1468 Zomba (2)	0	12.5	12.5	35
1929 Kollaa	0	12.5	0	12.5
2045 Peking (1)	0	12.5	0	12.5
2045 Peking (2)	0	12.5	12.5	35
2371 Dimitrov	12.5	35	12.5	35
2442 Corbett	12.5	35	12.5	35
2511 Patterson	0	12.5	0	12.5
2566 Kirghizia	0	12.5	0	12.5
2579 Spartacus	0	12.5	12.5	35
2653 Principia (1)	12.5	35	12.5	35
2653 Principia (2)	0	12.5	0	12.5
2653 Principia (3)	12.5	35	12.5	35
2763 Jeans (1)	0	12.5	0	12.5
2763 Jeans (2)	12.5	35	12.5	35
2763 Jeans (3)	0	12.5	0	12.5
2795 Lepage	0	12.5	0	12.5
2823 van der Laan	12.5	35	12.5	35
2851 Harbin (1)	0	12.5	0	12.5
2851 Harbin (2)	12.5	35	0	12.5
2912 Lapalma	12.5	35	12.5	35
3155 Lee (1)	12.5	35	0	12.5
3155 Lee (2)	12.5	35	0	12.5
3657 Ermolova	60	100	35	100
3703 Volkonskaya	0	12.5	0	12.5
3782 Celle	0	12.5	0	12.5
4038 Kristina	0	12.5	0	12.5
4215 Kamo (1)	0	12.5	0	12.5
4215 Kamo (2)	0	12.5	0	12.5
4215 Kamo (3)	0	12.5	0	12.5
4215 Kamo (4)	0	12.5	0	12.5
4796 Lewis	35	100	12.5	35
5111 Jacliff	0	12.5	0	12.5
5481 Kiuchi	12.5	35	0	12.5
5498 Gustafsson	12.5	35	12.5	35
7800 Zhongkeyuan	0	12.5	12.5	35
9481 Menchu	35	100	35	100
9553 Colas	60	100	60	100
16416	0	12.5	12.5	35
26886	60	100	60	100
27343 Deannashea	60	100	60	100
33881	60	100	35	100
36412	35	100	60	100
38070	12.5	35	35	60
50098	0	12.5	12.5	35
97276	0	12.5	12.5	35

Table 2
Particle size range of Group 2 selected from Fig. 5. Minimum and maximum value are defined by the two closest lines to the position of asteroid in scatterplot (Fig. 5).

	BDI versus BDII		HWHM versus BDII	
Name	min (μm)	min (μm)	min (μm)	max (μm)
5754	12.5	35	12.5	35
6331	0	12.5	0	12.5
15237 (1)	0	12.5	0	12.5
15237 (2)	12.5	35	0	12.5
17469	60	100	35	100
19165	35	100	35	100
29796	60	100	35	100
30872	0	12.5	0	12.5
32940	60	100	35	100
Amytis	35	100	35	100
Feldberg (1)	0	12.5	12.5	35
Feldberg (2)	12.5	35	12.5	35
Incidentia (1)	35	100	35	100
Incidentia (2)	12.5	35	12.5	35
Jeanloup	35	100	35	100
Kanatsu	35	100	35	100
Kourakuen	12.5	35	12.5	35
Kuga	0	12.5	12.5	35
Rotaryusa	35	100	35	100
Ruff	35	100	35	100
Shiretoko	12.5	35	12.5	35
Stohl (1)	0	12.5	0	12.5
Stohl (2)	0	12.5	0	12.5
Swope (1)	12.5	35	12.5	35
Swope (2)	0	12.5	12.5	35
Swope (3)	12.5	35	12.5	35
Veteraniya	0	12.5	0	12.5

Table 3
Sample and related particle size, modal mineral abundances and reference to optical constants retrieval for the endmembers used in the Hapke retrieval.

Name	Particle size (μm)	Wo (% mol)	Fs (% mol)	En (% mol)	References
Pigeonite	0–45	5	38	57	RELAB: DL -CMP -008 -A/C1DL08A
DL -CMP -025 -A	0–45	0	65	35	RELAB: DL -CMP -025 -A/C1DL25A
Hypersthene	45–90	3.6	41.5	54.9	RELAB: SC -EAC -036/C1SC36
Enstatite	45–75	1	12	87	RELAB: PE -CMP -031/C1PE31
Diopside	45–75	46	9	46	RELAB: PP -CMP -022/C1PP22
Anorthite	37–63	–	–	–	RELAB: MT -CMP -066/C1MT66
Olivina (Fo70)	0–45	–	–	–	RELAB: DD -MDD -039/C1DD39
Troilite	0–25	–	–	–	RELAB: MB -CMP -006 -1/CAMB06
Murchison	0–45	–	–	–	Cloutis et al., 2013

where b and c are constants that indicate the degree of scattering respectively backward/forward. Anyway, we can consider the scattering approximated to be isotropic (e.g. Roush et al., 2005), therefore b and c are set to 0.

The reflection geometry is set by the measurement procedure of the Reflectance Experiment Laboratory (RELAB) at Brown University, where the endmember spectra were obtained. This geometry is bidirectional with a 30° incidence angle and a 0° emission angle for a phase angle of 30°. Thus, the opposition surge that occurs at low phase angles is not important for our purposes, and the backscatter function is set to zero.

For a V-type asteroid the reflection geometry is probably not the same as for the laboratory sample end -member, due to their locations in the main asteroid belt and the resulting orbital geometry.

Most of the asteroids considered in this work are observed under a phase angle mainly between 10° and 20°. By assuming that the V-type photometric behaviour is similar to that of Vesta's bright regions (composed of HED, with a very low amount of dark materials) and by applying the phase functions obtained for Vesta by Longobardo et al. (2014), we obtained that the normalized reflectance variations in this phase angle interval are comparable with the spectral noise as found by Moskovitz et al., 2010. Therefore, variations in the asteroid spectra due to differences in observation phase angle are not expected to be more important than the signal to noise uncertainties of the observation, and can thus be neglected.

Accordingly, a number of spectra of mineral endmembers from RELAB database are selected and the optical constants of these end -members are retrieved. To estimate them, we have used the computational tool created by Ted Roush and used in (Roush et al., 2005) to

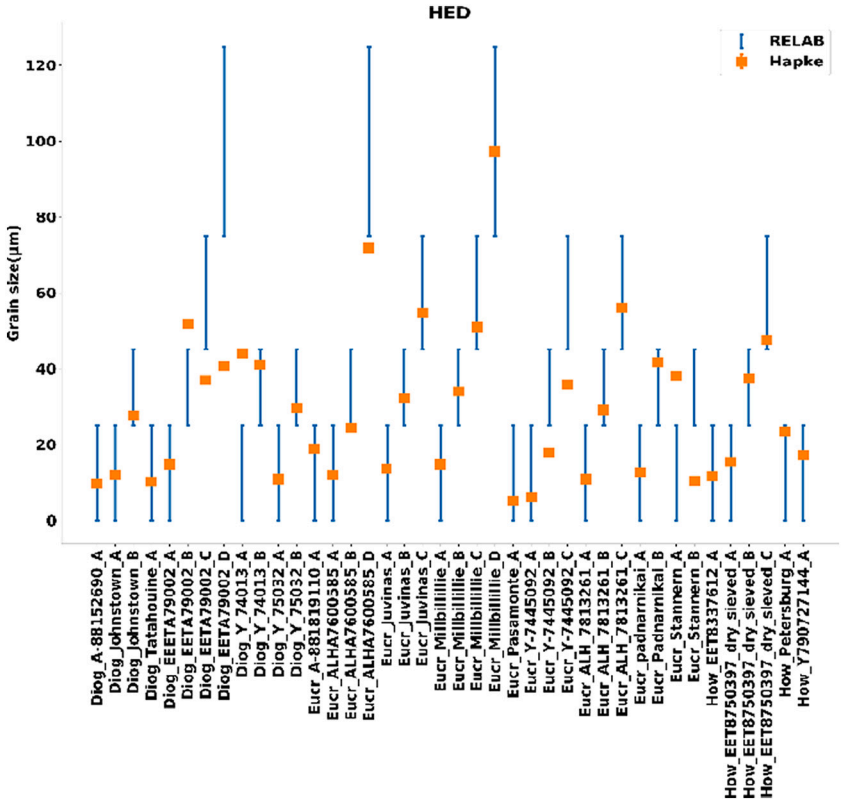

Fig. 6. Comparison between measured and modelled particle sizes for diogenite, eucrite and howardite meteorites. The subscript A,B,C,D close the name stands for particle size range: 0 -25, 25 -45, 45 -75, 75 -125 μm.

retrieve the extinction coefficient k. Then, each endmember reflectance spectrum is converted to its equivalent single -scattering albedo spectrum. Using Hapke's equation to mix the single scattering albedos from different endmembers, a reflectance spectrum can be generated. By varying particle size and mass fraction of selected endmembers, it is possible to search for the model mixture spectrum that best fits a given asteroid spectrum.

4. Calculation

4.1. Scatterplot analysis

To extract the spectral parameters (BC, BD, HWHM) we applied on V-type asteroids spectral data and on HED meteorites the spectroscopic methods explained in section 3.1. Although asteroids spectra are normalized to a specific wavelength, the HED spectra are not. We plot the HED spectral parameters without normalizing their spectra, because the variations that could cause are smaller than the error assumed for HED's unnormalized spectral parameters. For the same reason described above, lack of VIS wavelength data does not result in a significant error on the calculated parameters.

Pyroxenes are the most important mineral component of HED and V-type asteroids and show a strongly featured spectrum. Indeed, using a scatterplot of band I versus band II centers (hereafter BCI versus BCII) (Fig. 4), we can distinguish different lithologies on HED and then on V-type asteroids. Band I and band II centres are at shorter wavelengths for diogenites than for eucrites, as a consequence of more Mg -rich pyroxenes with lower Ca concentrations (Klima et al., 2008Cloutis et al., 1986). In Fig. 4 (right), group 1 spans from diogenitic to eucritic composition whereas group 2 shows a prevalence of mineralogy of howardite - diogenitic as described in literature (Hardersen et al., 2014, 2015, 2018). This difference between the two groups is not significant. In any case, their composition is similar to HED and therefore to Vesta. Furthermore, in Fig. 4 (right) group 1 has BCII that shifts to a smaller wavelength with respect to what reported in Moskovitz et al., 2010. We ascribe this offset to the different methodology to calculate BCII. Moskovitz et al. (2010) defines BCII as equal to the band II minima (without dividing out a continuum slope), while in this work, we consider BCII after removing the continuum.

In order to evaluate the particle size range of asteroids regolith (at least the interval of optical dominant particle size) and of HED, spectral parameters as Band depth I versus Band depth II (Fig. 5, left) and half width half maximum dextrum versus band depth II (Fig. 5, right) are plotted. However, in order to have a close comparison with the typical Vestan material, in these last scatterplots we selected only eucrite and howardite samples, omitting diogenite samples, as the diogenitic material is more sporadic on Vesta (e.g. De Sanctis et al., 2013). Fig. 5 shows how an increase in particle size produces an increase in band depth in HED meteorites. In particular, both Band I and Band II depths increase when particle size increases from 0 -25 to 75–125 μm. It seems that band depths become saturated at 85 μm (average of 45 -75 and 75 -125 μm, that is to say band depth is at a maximum for the larger particle sizes ranges (45–75, 75–125 μm), but none of this particle size consistently has the greatest band depth) consistent with previous studies of the behaviour of pyroxene absorption bands (Cloutis et al., 2013).

In both scatterplots, much of the asteroid's dataset seems located near particle size 0 -25 μm with none over the HED of 125 μm. De facto, on Vesta the regolith size domain appears to be <75 μm (Palomba et al., 2015, 2019; Gundlach and Blum, 2013; Hiroi et al., 1995) and the same seems to work for V-type asteroids too.

Thanks to these last two types of scatterplots, we can approximately infer the regolith particle size range for the V-type asteroids comparing with HED meteorites. Then, the particle size range selected for each asteroid is defined by the two closest lines to the position of asteroid in scatterplot (Fig. 5). When the scatterplots (Fig. 5 left and Fig. 5 right) give two different particle size ranges, the larger one is chosen (Table 1-

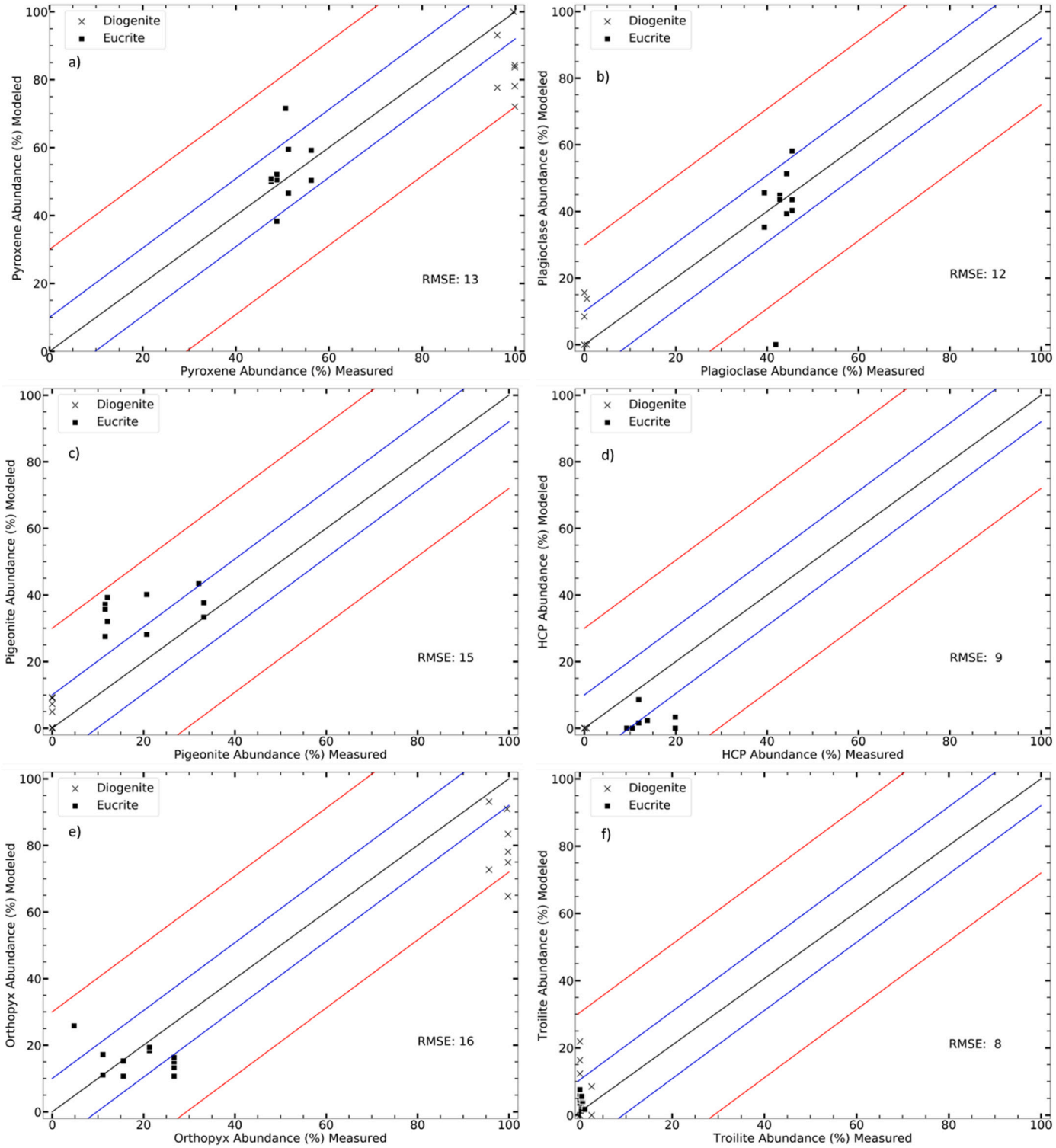

Fig. 7. Comparison of the Modelled (from Hapke RTM) and Measured (Mittlefehldt et al. (2015)) of the modal mineralogy estimated for Diogenite (cross) and Eucrite (square) from our sample suite (Table 4). The blue and red lines stand for ±10% and ± 30% from the literature modal mineralogy (black line). (a) Pyroxene; (b) Plagioclase; (c) Pigeonite; (d) High calcium pyroxene; (e) Orthopyroxene; (f) Troilite. (For interpretation of the references to colour in this figure legend, the reader is referred to the web version of this article.)

2).

In particular, the variability observed between multiple observations (connected with a line in Fig. 4-5) of individual asteroids is ascribed to a combination of compositional and particle size variations across the surface of the asteroids, differences in observing circumstances and uncorrected systematic effects.

4.2. *Input to Hapke radiative transfer model*

To evaluate the performance of the Hapke retrieval, we have first tested it on HED spectral sample measured particle size (taken from RELAB) and known composition from (Mittlefehldt et al., 2015). In particular, based on the results obtained in the scatterplot analysis, to

Table 4
Hapke model fractional mass (%) and particle size (μm) obtained for a suite of HED.

Name	R^2	CC (%)	Tr (%)	Ol (%)	Pl (%)	Diop (%)	Enst (%)	Hyp (%)	Ortho (%)	Pig (%)	Gs (μm)
Diogenite Johnstown 0 -25	0.997	0	9	0	14	0	68	1	4	5	12
Diogenite Johnstown 25 -45	0.998	5	0	2	0	0	75	10	7	0	28
Diogenite Tatahouine 0 -25	0.978	0	0	0	0	0	90	0	0	9	10
Diogenite EEETA79002 0 -25	0.990	0	7	0	8	0	70	5	0	9	15
Diogenite EETA79002 25 -45	0.980	0	12	0	16	0	50	14	0	7	52
Diogenite EETA79002 45 -75	0.983	0	16	0	0	0	50	34	0	0	37
Diogenite EETA79002 75 -125	0.952	0	22	0	0	0	40	38	0	0	41
Eucrite Juvinas 0 -25	0.996	0	2	0	51	0	18	0	0	28	14
Eucrite Juvinas 25 -45	0.995	0	1	0	39	0	8	11	0	40	32
Eucrite Juvinas 45 -75	0.991	0	0	0	36	0	1	18	0	45	55
Eucrite Millbillillie 0 -25	0.997	0	4	0	58	0	10	0	0	28	15
Eucrite Millbillillie 25 -45	0.992	0	6	0	44	0	1	12	0	37	34
Eucrite Millbillillie 45 -75	0.986	0	8	0	40	0	0	15	0	37	51
Eucrite Millbillillie 75 -125	0.961	0	4	0	44	0	0	16	0	36	97
Eucrite Pasamonte 0 -25	0.999	0	2	27	0	2	15	10	0	43	5
Eucrite Padnarnikai 0 -25	0.998	0	5	0	35	9	17	0	0	33	13
Eucrite Padnarnikai 25 -45	0.998	0	4	0	46	2	8	3	0	38	42
Eucrite Stannern 0 -25	0.999	0	6	0	44	3	15	0	0	32	10
Eucrite Stannern 25 -45	0.994	0	5	0	45	0	4	7	0	39	38

simulate asteroids spectra, we used the main endmembers of HED and we also added a darkening agent to find possible correlations between V-type asteroids and dark regions on Vesta (Palomba et al., 2014).

The used darkening agent is Murchison spectrum, a CM2 carbonaceous chondrite (from Cloutis et al., 2013). XRD modal analysis indicates that the Murchison CM2 chondrite consists of 15.1 vol% olivine, 8.3 vol% enstatite, 1.2 vol% calcite, 1.1 vol% magnetite, 0.7 vol% pentlandite, 1.2 vol% pyrrhotite, 50.3 vol% Fe -cronstedtite, and 22.2 vol% Mg -serpentine (Cloutis et al., 2013).

So, the selection of the end -members (main mineral components of HED and Murchison, Table 3) in the Hapke retrieval can be crucial to identify the correct composition of the body under analysis. In order to find the best fit, we could mix a large number of end -members, but this may require excessive computational time and resources, since all the combinations of end -members, mass fractions and particle size should be tested. Moreover, a large number of end -member could give rise to an overfitting model. Therefore, we selected as endmembers Murchison, Olivine (Fo_{90}) and Troilite as minor phases, a sample of plagioclase (Anorthite) and five pyroxenes: Diopside (as high calcium pyroxene), Pigeonite (as low calcium pyroxene), Enstatite (orthopyroxene Magnesium rich), hypersthene and a ferrous rich orthopyroxene (Table 3).

In addition, the created particle size for each mixture was varied from 1 μm up to a limit of 125 μm, in agreement with our spectroscopic analysis (Fig. 4-5) and previous studies on regolith particle size of Vesta and V-type asteroids (Palomba et al., 2014, 2019; Gundlach and Blum, 2013; Hiroi et al., 1995). This constrains the Hapke model from producing degenerate results. In other words, to find the best fit, Hapke retrieval must balance reflectance (i.e., abundance of minerals as results) and band depth (i.e., the particle size results) (Lucey, 1998). This could give an overestimation/underestimation of particle size and/or modal abundance (that counterbalance each other).

The results obtained from the model mixing procedure on HED give a really good result. On a sample of 40 HED with a defined particle size range, 31 of them are correctly modelled in their literature particle size range by the Hapke radiative model (Fig. 6). So, we assume, as error on the particle size resulted from Hapke retrieval, the standard deviation of the discrepancies between the modelled particle sized and the mean value of particle size from the defined particle size range. We calculated them of HED with absolute and normalized spectra and we obtained a value of ±12, 17 and 21 μm (error for absolute spectra, spectra normalized at 1.5 μm and spectra normalized at 1.215 μm).

Comparing modal composition of Hapke model to the HED with known composition from (Mittlefehldt et al., 2015) (Fig. 7), the model is capable to estimate the abundance of Pyroxene, Orthopyroxene, Pigeonite and High Calcium Pyroxene to within ≈ ±30% and of Plagioclase to within ≈ ± 20% except for eucrite Pasamonte, of Troilite to within ≈ ± 10% except for diogenite EEETA79002 and of Olivine ≈ ± 2% except for eucrite Pasamonte (Table 4). The same procedure has been made also for HED normalized spectra and we obtained discrepancies from the known composition similar or less than the previous described above. So, we assume the value obtained above as maximum error of modal composition resulted from Hapke retrieval on asteroids.

4.3. Application of Hapke model on asteroids dataset

The ability of the Hapke RTM to predict the modal mineralogy abundance and the particle size HED here used makes it suitable to model composition and particle size of V-type asteroids.

To prevent possible degeneration in the creation of synthetic spectra of V-type asteroids, we used scatterplots results where we inferred the regolith particle size range for each asteroid and used it as input to Hapke model. The result of Hapke retrieval is shown in Table 5 and in Table 6 for group 1 and group 2 of asteroids respectively. Spectral fits of the asteroid's dataset are robust with a global R mean square of 0.98. Retrieved particle sizes are very small with a mean value of 20 μm.

Asteroid 2579 Spartacus modal mineralogy is consistent with the presence of olivine. It was suspected before (Moskovitz et al., 2010; Burbine et al., 2001) through spectroscopic analysis (i.e., band ratio and band centre analysis). It could be due to an origin from deep within the Vesta parent body where olivine abundances were higher, or to its origin on another parent body (Moskovitz et al., 2010).

From Hapke retrieval, Asteroid 809 Lundia seems to have a diogenitic mineralogy with a modal particle size of 35 μm (range of 35 -100 μm from spectroscopic results) in accordance with the previous analysis by Birlan et al. (2014). He investigated the VNIR spectral region of Lundia with meteorites from RELAB database, and he found that it was mostly howarditic and diogenitic with particle size <100 μm.

Lim et al. (2011) made analysis of near -IR spectra of 956 Elisa with the Modified Gaussian Model that outcomes in two pyroxene compositions (75% magnesian low -Ca pyroxene and 25% high -Ca pyroxene), while analysing the diagnostic 9–12 μm features in the Mid -IR these are better fit by a mixture of diogenite and 10–15% olivine (e.g. olivine diogenite) than by a mixture that includes cumulate eucrites. In our work, we have two near -IR spectra collected in two different dates with the same telescope. In the first spectrum, Hapke retrieval gives a modal composition of 78% low -Ca pyroxene (orthopyroxene) and 22% high -Ca pyroxene (diopside and pigeonite) in accordance with the results of Lim et al. (2011). The second spectrum is characterized by the presence

Table 5
Hapke model fractional mass (%) and particle size (μm) obtained on group 1 asteroids dataset. The particle size range obtained from scatterplot analysis and the V-type family are also shown.

Name	R^2	CC (%)	Tr (%)	Olv (%)	Pl (%)	Diop (%)	Enst (%)	Hyp (%)	Ortho (%)	Pige (%)	Gs (μm)	Gs_range (μm)	Family
809 Lundia	0.998	8	0	0	6	23	27	18	17	0	35	35 -100	FUGITIVE
956 Elisa (1)	0.997	0	1	0	0	20	42	29	8	2	13	12.5 -100	FUGITIVE
956 Elisa (2)	0.992	0	18	0	12	3	20	40	0	6	35	35 -100	FUGITIVE
1468 Zomba (1)	0.996	1	1	0	0	30	28	23	9	8	13	0 -12.5	IOs
1468 Zomba (2)	0.988	0	0	10	0	30	37	0	23	0	10	0 -35	IOs
1929 Kollaa	0.995	0	0	0	0	23	33	24	6	14	10	0 -12.5	VESTOIDS
2045 Peking (1)	0.990	0	0	0	0	31	0	56	10	3	6	0 -12.5	VESTOIDS
2045 Peking (2)	0.996	0	7	16	0	18	31	10	18	0	20	0 -35	VESTOIDS
2371 Dimitrov	0.970	0	1	0	11	20	30	26	0	11	13	12.5 -35	LOW -I
2442 Corbett	0.995	0	0	0	45	3	24	17	3	9	35	12.5 -35	LOW -I
2511 Patterson	0.995	0	0	0	0	21	42	20	14	3	8	0 -12.5	VESTOIDS
2566 Kirghizia	0.964	0	0	0	1	0	1	75	0	23	3	0 -12.5	LOW -I
2579 Spartacus	0.982	0	0	19	0	25	2	30	4	20	8	0 -35	FUGITIVE
2653 Principia (1)	0.994	0	0	0	43	4	18	16	3	15	35	12.5 -35	LOW -I
2653 Principia (2)	0.992	0	0	0	2	22	1	53	6	15	5	0 -12.5	LOW -I
2653 Principia (3)	0.992	0	0	0	51	2	14	10	0	23	35	12.5 -35	LOW -I
2763 Jeans (1)	0.994	0	0	1	0	28	0	40	0	31	4	0 -12.5	LOW -I
2763 Jeans (2)	0.987	0	2	0	18	31	17	8	24	0	13	12.5 -35	LOW -I
2763 Jeans (3)	0.993	0	1	0	0	37	22	14	16	10	7	0 -12.5	LOW -I
2795 Lepage	0.990	0	0	0	0	1	1	78	1	19	3	0 -12.5	FUGITIVE
2823 Van der Laan	0.955	0	0	10	37	1	23	10	0	19	35	12.5 -35	LOW -I
2851Harbin (1)	0.996	0	0	10	0	0	52	32	0	6	9	0 -12.5	IOs
2851Harbin (2)	0.998	2	0	7	0	11	50	24	6	0	18	0 -35	IOs
2912 Lapalma	0.997	0	0	0	0	17	46	26	10	0	14	12.5 -35	FUGITIVE
3155 Lee (1)	0.900	0	0	0	0	0	0	100	0	0	6	0 -35	VESTOIDS
3155 Lee (2)	0.986	0	0	0	0	0	70	23	0	7	8	0 -35	VESTOIDS
3657 Ermolova	0.982	0	24	4	11	0	14	41	0	6	35	35 -100	VESTOIDS
3703 Volkonskaya	0.982	0	0	0	0	27	45	11	17	1	5	0 -12.5	VESTOIDS
3782 Celle	0.974	0	0	0	0	11	70	2	6	11	7	0 -12.5	VESTOIDS
4038 Kristina	0.984	0	0	0	0	20	46	11	16	6	3	0 -12.5	VESTOIDS
4215 Kamo (1)	0.985	0	0	0	2	9	50	19	12	8	4	0 -12.5	VESTOIDS
4215 Kamo (2)	0.984	0	0	0	2	0	35	43	0	20	2	0 -12.5	VESTOIDS
4215 Kamo (3)	0.977	0	0	1	0	2	6	67	0	23	2	0 -12.5	VESTOIDS
4215 Kamo (4)	0.961	0	0	8	0	17	50	0	24	0	5	0 -12.5	VESTOIDS
4796 Lewis	0.979	0	0	0	53	0	15	15	6	11	50	12.5 -100	LOW -I
5111 Jacliff	0.996	0	1	1	0	19	51	12	16	0	5	0 -12.5	VESTOIDS
5481 Kiuchi	0.973	0	0	8	1	17	42	15	16	0	13	0 -35	VESTOIDS
5498 Gustafsson	0.997	0	0	0	35	16	23	10	6	9	28	12.5 -35	LOW -I
7800 Zhongkeyuan	0.939	0	0	9	0	27	49	0	15	0	10	0 -35	LOW -I
9481 Menchu	0.937	0	0	0	65	0	0	34	0	1	35	35 -100	LOW -I
9553 Colas	0.995	0	0	0	41	4	26	21	0	8	60	60 -100	LOW -I
16416	0.966	0	0	0	0	44	0	36	20	0	6	0 -35	FUGITIVE
26886	0.949	0	1	0	40	0	27	30	0	2	60	60 -100	LOW -I
27343 Deannashea	0.991	8	1	6	12	5	34	26	7	0	60	60 -100	LOW -I
33881	0.992	0	16	0	11	8	22	31	0	11	43	35 -100	IOs
36412	0.974	0	1	1	29	19	12	29	7	2	35	35 -100	LOW -I
38070	0.979	0	0	3	63	4	11	12	0	8	60	12.5 -60	IOs
50098	0.987	0	0	0	0	0	1	87	0	12	5	0 -35	VESTOIDS
97276	0.928	0	0	0	0	0	0	65	0	34	2	0 -35	LOW -I

of Troilite, in particular a 18% of Troilite, 60% low -Ca pyroxene (orthopyroxene) and 9% high -Ca pyroxene (diopside and pigeonite). However, we suppose that when an asteroid was observed more than once and there is variation issue from model, this could be caused by a combination of compositional variation across the surface of the asteroids, differences in observing circumstances and uncorrected systematic effects. The first possibility could be tested if the sub -observer latitude and longitude were known for each asteroid showing variations across the surface.

4.4. Statistical analysis on V-type family

Dynamical subclasses of V-type population are thought to have been created at the epoch of the Vesta family formation and migrated to their current position via some still unknown dynamical mechanisms.

Thus, there is a possible chronologic link between impact events on Vesta and the Vestoids that are thought to have eventually supplied the HEDs to nearby escape hatches from the Main Belt. We use the results of modal mineralogy from Hapke retrieval techniques (Fig. 8) and the HED literature to look for statistically significant differences among the spectral properties of V-type asteroids belonging to different dynamical subclasses. Mittlefehldt et al. (2015) show the igneous and breccia lithologic types and modal mineralogy of HED. In particular, we can distinguish diogenites (approximately 100% of pyroxene), noritic diogenites (2 -42% plagioclase, 52 -97 pyroxene), cumulate eucrite (30 -64% plagioclase and 36 -70% pyroxene), basaltic eucrite (39 -46% plagioclase, 46 -60% pyroxene). Then, in Table 7 we report the mean and the standard deviation of sample of the four subclasses (Fugitive, Vestoids, Inner Others and Low -i). It seems that Vestoids and Fugitive are diogenitic (diogenitic and noritic diogenites respectively), while Low -I and Inner Other (IOs) are eucritic. Furthermore, in all the family, the model does not identify any presence of Carbonaceous Chondrites (Murchison column of Table 7),.

Table 6
Hapke model (with more constrains) of fractional mass (%) and particle size (μm) obtained on group 2 asteroids dataset. The particle size range obtained from scatterplot analysis and the V-type family are also shown.

Name	R^2	CC (%)	Tr (%)	Olv (%)	Pl (%)	Diop (%)	Enst (%)	Hyp (%)	Ortho (%)	Pige (%)	Gs (μm)	Gs_range (μm)	Family
5754	0.991	1	0	3	45	2	23	14	5	8	26	12.5 -35	IOs
6331	0.976	1	1	0	0	13	52	25	8	0	4	0 -12.5	VESTOIDS
15237 (1)	0.982	0	0	0	0	8	68	2	10	11	6	0 -12.5	VESTOIDS
15237 (2)	0.955	0	0	0	1	0	50	29	15	5	4	0 -35	VESTOIDS
17469	0.995	1	1	0	33	2	32	29	0	3	35	35 -100	VESTOIDS
19165 Nariyuki	0.993	0	0	0	52	1	14	13	3	17	36	35 -100	FUGITIVE
29796	0.988	2	1	0	28	3	33	23	0	11	36	35 -100	IOs
30872	0.968	0	0	0	0	20	0	63	1	15	3	0 -12.5	LOW -i
32940	0.975	9	0	0	14	0	36	24	1	16	35	35 -100	FUGITIVE
5560 Amytis	0.983	0	0	0	27	12	33	21	5	2	35	35 -100	FUGITIVE
10666 Feldberg (1)	0.969	0	0	6	0	0	3	52	24	14	3	0 -35	FUGITIVE
10666 Feldberg (2)	0.988	0	0	0	49	6	17	11	10	6	16	12.5 -35	FUGITIVE
3849 Incidentia (1)	0.992	0	1	0	51	8	9	11	1	18	35	35 -100	LOW -i
3849 Incidentia (2)	0.988	0	0	0	58	3	8	9	0	21	35	12.5 -35	LOW -i
5235 Jeanloup	0.996	0	0	0	47	5	27	7	1	13	52	35 -100	IOs
6976 Kanatsu	0.993	0	2	0	37	5	20	25	0	11	35	35 -100	IOs
9147 Kourakuen	0.989	0	0	0	31	10	31	16	7	5	14	12.5 -35	FUGITIVE
5875Kuga	0.975	0	0	0	0	1	0	43	15	41	3	0 -35	IOs
31414 Rotaryusa	0.986	6	0	1	20	4	43	19	5	3	35	35 -100	IOs
8149 Ruff	0.993	0	4	0	38	3	23	19	3	9	38	35 -100	IOs
3867 Shiretoko	0.995	0	0	0	28	30	17	1	13	10	21	12.5 -35	IOs
3715 Stohl (1)	0.985	0	0	0	8	14	0	52	1	25	3	0 -12.5	LOW -i
3715 Stohl (2)	0.986	0	0	4	0	27	2	49	0	18	4	0 -12.5	LOW -i
2168 Swope (1)	0.983	1	0	0	13	16	29	30	11	0	13	12.5 -35	LOW -i
2168 Swope (2)	0.963	0	0	11	0	3	0	65	21	0	3	0 -35	LOW -i
2168 Swope (3)	0.977	0	0	0	21	12	43	11	9	4	13	12.5 -35	LOW -i
2011 Veteraniya	0.978	0	0	0	3	0	0	55	0	41	2	0 -12.5	VESTOIDS

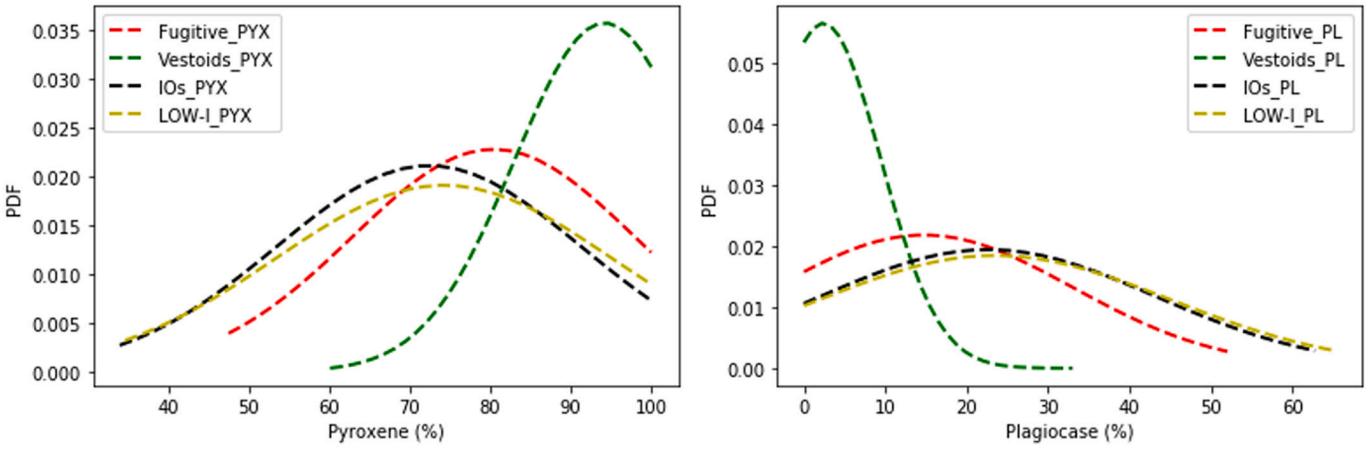

Fig. 8. Probability density function of Pyroxene (left) and of Plagioclase (right) for each V-type family subclass. Function calculated from scipy.stats library of Pyhton.

Table 7
Results of mean mineralogy for each subclass from Hapke retrival.

	Pyroxene (%)	Plagioclase (%)	Murchison (%)	Number of spectra	Possible mineralogy
FUGITIVE	80 ± 18	15 ± 18	1 ± 3	13	Noritic diogenites
VESTOIDS	94 ± 11	2 ± 7	0	22	Diogenitic
IOs	72 ± 19	23 ± 21	1 ± 1	14	Eucritic
LOW -i	74 ± 21	23 ± 22	0 ± 2	27	Eucritic

5. Discussion

Studying the mineralogy and the dynamic of V-type population, we can retrace the evolution history of Vesta. Marchi et al. (2012), while studying the collision history of Vesta, found that the density of craters increases from the Rheasilvia rim to northern latitudes. This dichotomy in terms of crater density indicates that heavily cratered terrains (centered at about 348°E, 17°N and 110°E, 17°N) are much older than Rheasilvia basin, whose most probable age is estimated to be 1.0 ± 0.2 Ga (Marchi et al., 2012). Furthermore, De Sanctis et al., 2012 based on data obtained by the Dawn spacecraft's VNIR spectrometer found that Rheasilvia basin is consistent with a greater proportion of diogenite on the surface in this deeply excavated region, while spectra from the equatorial regions are consistent with a greater eucrite component. Thus, there is a possible chronologic link between impact events on Rheasilivia crater and the Vestoids which, from our work, have a mineralogy associated to Diogenites. For Fugitive, the better match is with a diogenitic composition. For this subclass, Nesvorny et al. (2008) has estimated the probable age of formation is in ~1–2 Gy or they must have been liberated from Vesta much earlier than ~2 Gy ago then, it is

possible, that they were ejected in an older (2 Ga) cratering event that produced the Veneneia basin that underlies Rheasilvia (McSween et al., 2013). The most 'ancient' family, that is Low -i asteroids (they may date back to the Late Heavy Bombardment (LHB) epoch or even to the 4.48 -Ga impact on Vesta), seems to have a eucritic composition compatible with a possible scenario where this family were formed by a collision in which the outermost eucritic layer of Vesta (in the recent models e.g. De Sanctis et al., 2012; Barrat et al., 2010, Vesta is supposed to have a eucritic crust) were ejected.

In any family, there is no signature of dark material as carbonaceous chondrites (here we used Murchison spectra to simulate it).

The presence of olivine in 2579 Spartacus asteroid, as suspected before by Burbine et al., 2001 and Moskovitz et al., 2010, gives rise to various alternative scenarios of olivine traces on Vesta, as well to the existence of another parent body that could have generated the V-type asteroids. The alternative models of Vesta indicate that deep cumulates originated during the cooling of the magma ocean which underwent extensive remelting, forming diogenitic intrusions (plutons) within the massive eucritic crust (Yamaguchi et al., 2011; Barrat et al., 2010; Shearer et al., 2010). The existence of such crustal plutons could fit the scattered patches of olivine -rich material found in Palomba et al. (2015) and Ruesch et al. (2014). A final possibility that has been recently proposed is that most of the olivine identified on the Vesta surface could be the result of exogenous delivery by olivine -rich impactors instead of mantle excavation (Turrini et al., 2016; Le Corre et al., 2015). The limited number of olivine enrichments on Vesta and their association to post -Rheasilvia craters not capable to excavate the crust are actually consistent with this possibility, as impacts of A -type asteroids from Rheasilvia's formation to now are in principle capable to supply enough events to explain the two most olivine -rich sites Arruntia and Bellicia, and all the additional less olivine -rich sites (Turrini et al., 2016).

If Spartacus could be fragments of basaltic crust from a non -Vestoid differentiated parent body, it could be spectroscopically distinct from the Vesta. So, it is more likely it could be due to an origin from Vesta where olivine abundances were higher (in the patches of olivine -rich materials, Palomba et al., 2015).

6. Conclusions

The composition of the regolith particle size of groundbased 76 VIS -NIR normalized spectra of V-type asteroids, has been investigated and a new approach of analysis, i.e., a combination of spectroscopic analysis and Hapke radiative transfer model has been proposed. In particular, the obtained information from the scatterplot analysis (Fig. 4-5) is used as constrain in the Hapke's bidirectional reflectance model to retrieve modal composition and particle size information for each V-type asteroid. Spartacus asteroid seems to have a modal mineralogy consistent with the presence of olivine as suspected before (Moskovitz et al., 2010; Burbine et al., 2001). This could be due to an origin from region of Vesta where olivine abundances were higher, or it could be due to its origin on another parent body that could have gone through the same thermal evolution as Vesta.

The dataset was divided in Group 1 and Group 2, basing on their previous normalization of data (Moskovitz et al., 2010, Hardersen et al. (2014, 2015, 2018)) however, in our analysis, they do not show significant difference in composition and particle size. The results of modal mineralogy from Hapke retrieval techniques are used to look for statistically significant differences among the spectral properties of V-type asteroids belonging to different dynamical subclasses because there is a possible chronologic link between impact events on Vesta and the V-type family. The most ancient V-type family, e.g. Low -I asteroids (they may date back to the Late Heavy Bombardment (LHB) epoch or even to the 4.48 -Ga impact on Vesta) has an eucritic composition compatible with an ejection of the outermost layer of Vesta. Then, the Fugitive V-type asteroid material were ejected in an older (2 Ga) cratering event that produced the Veneneia basin (McSween et al., 2013) (with asteroids forming ~1–2 Gy Ga ago, Nesvorny et al., 2008) and then there are the Vestoids family, whose dynamical parameters are still more similar to Vesta and is supposed to be the younger subclass of V-type family, that they could associate to Rheasilvia basin. The last two family seems to have a diogenitic composition compatible with that of the south of Vesta where the two huge craters are located.

In conclusion, the developed procedure could be a starting point to develop a new automatic analysis method similar to the widespread supervised machine learning methods which represent an opportunity to research the difference between the V-type family asteroids from mineralogy features. We hope to augment the database of V-type asteroids to improve the statistical analysis and to check if there are heterogeneities of each surface mineralogy comparing the different spectra of the same asteroids taken in different time with their shape model.

Declaration of Competing Interest

None.

Data availability

Data will be made available on request.

Acknowledgments

We warmly thank Beth Ellen Clark and Clark Chapman for the very constructive reviews which helped to improve our manuscript.

Appendix

Table 1
List of spectral parameters and their errors for HED suite.

Name	Particle size (μm)	BCI (μm)	BCII (μm)	BDI	BDII	HWHMI DX	Err BCI (μm)	Err BCII (μm)	Err BDI	Err BDII	Err HWHM I dx
Diogenite EEETA79002	0 -25	0.92	1.90	0.51	0.29	0.09	0.01	0.02	0.01	0.01	0.01
Diogenite EEETA79002	25 -45	0.92	1.89	0.64	0.44	0.10	0.01	0.02	0.01	0.01	0.01
Diogenite EEETA79002	45 -75	0.92	1.89	0.64	0.47	0.10	0.01	0.02	0.01	0.02	0.01
Diogenite EEETA79002	75 -125	0.92	1.90	0.61	0.47	0.11	0.01	0.01	0.01	0.01	0.01
Diogenite Y -74013	0 -25	0.93	1.91	0.42	0.24	0.09	0.01	0.01	0.01	0.01	0.01
Diogenite Y -74013	25 -45	0.93	1.91	0.60	0.42	0.10	0.01	0.01	0.01	0.01	0.01
Diogenite Y -75032	0 -25	0.93	1.94	0.52	0.29	0.10	0.01	0.01	0.01	0.01	0.01
Diogenite Y -75032	25 -45	0.93	1.94	0.66	0.46	0.11	0.01	0.01	0.01	0.01	0.01
Diogenite A -881526,90	0 -25	0.93	1.89	0.64	0.42	0.10	0.01	0.01	0.01	0.01	0.01

(continued on next page)

Table 1 (*continued*)

Name	Particle size (μm)	BCI (μm)	BCII (μm)	BDI	BDII	HWHMI DX	Err BCI (μm)	Err BCII (μm)	Err BDI	Err BDII	Err HWHM I dx
Diogenite Johnstown	0 -25	0.92	1.89	0.45	0.24	0.10	0.01	0.01	0.01	0.01	0.01
Diogenite Johnstown	25 -45	0.92	1.89	0.63	0.44	0.11	0.01	0.01	0.01	0.01	0.01
Diogenite Tatahouine	0 -25	0.93	1.89	0.63	0.41	0.10	0.01	0.02	0.01	0.01	0.01
Eucrite ALH78132,61	0 -25	0.94	1.95	0.43	0.26	0.09	0.01	0.01	0.01	0.01	0.01
Eucrite ALH78132,61	25 -45	0.94	1.95	0.58	0.41	0.10	0.01	0.02	0.01	0.01	0.01
Eucrite ALH78132,61	45 -75	0.94	1.95	0.62	0.48	0.11	0.01	0.01	0.01	0.01	0.01
Eucrite Padnarnikai	0 -25	0.94	1.99	0.47	0.26	0.11	0.01	0.01	0.01	0.01	0.01
Eucrite Padnarnikai	25 -45	0.94	1.98	0.55	0.37	0.13	0.01	0.02	0.01	0.01	0.01
Eucrite Stannern	0 -25	0.94	1.99	0.41	0.23	0.09	0.01	0.01	0.01	0.01	0.01
Eucrite Stannern	25 -45	0.94	1.99	0.52	0.38	0.11	0.01	0.01	0.01	0.01	0.01
Eucrite A -881819,110	0 -25	0.94	1.96	0.48	0.28	0.10	0.01	0.01	0.01	0.01	0.01
Eucrite ALHA76005,85	0 -25	0.94	1.97	0.39	0.23	0.09	0.01	0.02	0.01	0.01	0.01
Eucrite ALHA76005,85	25 -45	0.94	1.96	0.49	0.35	0.10	0.01	0.01	0.01	0.01	0.01
Eucrite ALHA76005,85	75 -125	0.94	1.96	0.53	0.44	0.11	0.01	0.01	0.01	0.01	0.01
Eucrite Juvinas	0 -25	0.94	1.99	0.47	0.27	0.10	0.01	0.02	0.01	0.01	0.01
Eucrite Juvinas	25 -45	0.94	1.98	0.60	0.42	0.12	0.01	0.01	0.01	0.01	0.01
Eucrite Juvinas	45 -75	0.94	1.97	0.62	0.47	0.13	0.01	0.01	0.01	0.01	0.01
Eucrite Millbillillie	0 -25	0.94	1.99	0.45	0.24	0.11	0.01	0.01	0.01	0.01	0.01
Eucrite Millbillillie	25 -45	0.94	1.99	0.59	0.38	0.13	0.01	0.01	0.01	0.01	0.01
Eucrite Millbillillie	45 -75	0.94	1.99	0.60	0.41	0.14	0.01	0.01	0.01	0.01	0.01
Eucrite Millbillillie	75 -125	0.95	1.99	0.58	0.43	0.14	0.01	0.01	0.01	0.01	0.01
Eucrite Pasamonte	0 -25	0.94	1.99	0.49	0.29	0.12	0.01	0.01	0.01	0.01	0.01
Eucrite Y -74450,92	0 -25	0.94	1.97	0.38	0.19	0.10	0.01	0.02	0.01	0.01	0.01
Eucrite Y -74450,92	25 -45	0.94	1.96	0.53	0.33	0.12	0.01	0.02	0.01	0.01	0.01
Eucrite Y -74450,92	45 -75	0.94	1.97	0.57	0.39	0.13	0.01	0.01	0.01	0.01	0.01
Howardite EET83376,12	0 -25	0.94	1.96	0.46	0.29	0.09	0.01	0.01	0.01	0.01	0.01
Howardite EET87503,97_dry_sieved	0 -25	0.94	1.95	0.38	0.19	0.10	0.01	0.01	0.01	0.01	0.01
Howardite EET87503,97_dry_sieved	25 -45	0.94	1.95	0.45	0.28	0.10	0.01	0.01	0.01	0.01	0.01
Howardite EET87503,97_dry_sieved	45 -75	0.94	1.94	0.49	0.36	0.11	0.01	0.01	0.01	0.01	0.01
Howardite Petersburg	0 -25	0.94	1.96	0.44	0.27	0.10	0.01	0.03	0.01	0.01	0.01
Howardite Y790727,144	0 -25	0.94	1.95	0.49	0.31	0.09	0.01	0.01	0.01	0.01	0.01

Table 2
List of spectral parameters and their errors for V-type asteroids (group 1).

Name	BCI (μm)	BCII (μm)	BDI	BDII	HWHM_I_DX	err_BCI (μm)	err_BCII (μm)	err_BDI	err_BDII	err_HWHM_I_dx
809_080826t063534	0.93	1.92	0.47	0.39	0.10	0.01	0.01	0.01	0.01	0.01
956_080705t113501	0.93	1.95	0.46	0.39	0.09	0.01	0.02	0.05	0.01	0.01
956_081009t062401	0.92	1.89	0.49	0.43	0.10	0.01	0.01	0.05	0.01	0.01
1468_030930	0.93	1.98	0.36	0.33	0.08	0.01	0.02	0.01	0.01	0.01
1468_090426t080940	0.93	1.97	0.39	0.30	0.10	0.01	0.01	0.04	0.01	0.01
1929_010219t133209	0.94	1.95	0.34	0.36	0.08	0.01	0.01	0.02	0.01	0.01
2045_020114t055048	0.93	1.93	0.32	0.35	0.08	0.01	0.01	0.02	0.01	0.02
2045_080826t114547	0.93	1.93	0.37	0.33	0.09	0.01	0.01	0.02	0.01	0.01
2371_090801t125752	0.93	1.99	0.43	0.35	0.09	0.01	0.03	0.07	0.03	0.01
2442_020915t102739	0.93	1.94	0.36	0.39	0.07	0.01	0.01	0.03	0.01	0.01
2511_040507t080222	0.93	1.95	0.35	0.33	0.07	0.01	0.02	0.01	0.01	0.01
2566_020508t080611	0.93	1.94	0.35	0.35	0.08	0.01	0.01	0.01	0.01	0.01
2579_001010t053342	0.94	1.99	0.33	0.34	0.09	0.02	0.01	0.01	0.01	0.02
2653_021126t075114	0.93	1.96	0.39	0.42	0.07	0.01	0.01	0.01	0.01	0.01
2653_050716t104949	0.93	1.96	0.34	0.34	0.07	0.01	0.01	0.01	0.01	0.01
2653_080419t072808	0.94	1.97	0.38	0.37	0.07	0.01	0.01	0.01	0.01	0.01
2763_040626t074219	0.94	1.98	0.31	0.29	0.07	0.01	0.01	0.01	0.01	0.01
2763_080705t115918	0.94	1.93	0.42	0.30	0.10	0.01	0.02	0.03	0.01	0.01
2763_080826t080234	0.94	1.99	0.38	0.30	0.09	0.01	0.01	0.07	0.01	0.01
2795_050409t102202	0.94	1.94	0.29	0.35	0.07	0.01	0.01	0.01	0.01	0.01
2823_051122	0.93	1.93	0.40	0.40	0.08	0.02	0.01	0.05	0.01	0.01
2851_010824t122815	0.92	1.91	0.33	0.38	0.07	0.02	0.01	0.01	0.01	0.01
2851_030112t120154	0.93	1.93	0.35	0.39	0.07	0.01	0.01	0.01	0.01	0.01
2912_010220t110902	0.93	1.94	0.37	0.43	0.07	0.02	0.01	0.01	0.01	0.01
3155_010622t085308	0.92	1.92	0.36	0.39	0.07	0.01	0.01	0.02	0.01	0.01
3155_050714t113333	0.92	1.90	0.36	0.37	0.06	0.01	0.04	0.01	0.01	0.01
3657_090801t055723	0.93	1.89	0.48	0.45	0.10	0.01	0.01	0.01	0.01	0.01
3703_060603	0.92	1.95	0.28	0.28	0.07	0.03	0.01	0.02	0.01	0.01
3782_021126t122636	0.92	1.86	0.33	0.27	0.07	0.01	0.01	0.01	0.01	0.01
4038_021028	0.92	1.97	0.26	0.23	0.07	0.01	0.01	0.01	0.01	0.01
4215_021126t062437	0.93	1.93	0.33	0.28	0.07	0.01	0.01	0.02	0.01	0.01

(*continued on next page*)

Table 2 (*continued*)

Name	BCI (μm)	BCII (μm)	BDI	BDII	HWHM_I_DX	err_BCI (μm)	err_BCII (μm)	err_BDI	err_BDII	err_HWHM_I_dx
4215_050715t105742	0.93	1.97	0.28	0.26	0.07	0.01	0.02	0.01	0.01	0.01
4215_080419t075148	0.93	1.93	0.32	0.29	0.07	0.01	0.02	0.01	0.01	0.01
4215_090801t102437	0.93	1.94	0.31	0.24	0.07	0.01	0.04	0.02	0.03	0.01
4796_090109t050454	0.93	1.97	0.46	0.41	0.09	0.01	0.05	0.02	0.02	0.01
5111_050905	0.92	1.95	0.30	0.27	0.07	0.02	0.01	0.01	0.01	0.01
5481_090801t140554	0.93	1.91	0.38	0.35	0.07	0.01	0.02	0.01	0.03	0.03
5498_080826t102951	0.93	1.94	0.45	0.33	0.10	0.01	0.02	0.03	0.01	0.01
7800_090109t072049	0.92	1.81	0.39	0.26	0.11	0.01	0.01	0.03	0.05	0.01
9481_080826t092100	0.94	1.89	0.45	0.40	0.10	0.01	0.01	0.01	0.02	0.01
9553_090108t050025	0.93	1.90	0.53	0.44	0.11	0.01	0.01	0.01	0.01	0.01
16416_071123t082207	0.93	1.92	0.39	0.29	0.10	0.01	0.04	0.04	0.02	0.03
26886_080705t104114	0.92	1.88	0.49	0.51	0.09	0.01	0.01	0.03	0.02	0.01
27343_080826t071152	0.93	1.90	0.55	0.45	0.10	0.01	0.01	0.04	0.01	0.01
33881_071123t070955	0.93	1.88	0.54	0.42	0.10	0.01	0.01	0.03	0.01	0.01
36412_071123t060625	0.94	1.96	0.44	0.42	0.11	0.01	0.03	0.01	0.03	0.01
38070_061005t111826	0.94	1.97	0.44	0.32	0.13	0.01	0.03	0.03	0.02	0.02
50098_050904	0.93	1.95	0.32	0.40	0.08	0.02	0.01	0.01	0.01	0.02
97276_071123t095000	0.94	1.99	0.35	0.26	0.11	0.01	0.01	0.02	0.01	0.01

Table 3
List of spectral parameters and their errors for V-type asteroids (group 2).

Name	BCI (μm)	BCII (μm)	BDI	BDII	HWHM I DX	Err BCI (μm)	Err BCII (μm)	Err BDI	Err BDII	Err HWHM I dx
5754_2	0.93	1.88	0.40	0.34	0.09	0.01	0.01	0.10	0.02	0.01
6331	0.93	1.88	0.33	0.29	0.08	0.01	0.01	0.04	0.01	0.01
15237_1	0.92	1.90	0.38	0.30	0.07	0.02	0.01	0.12	0.01	0.01
15237_2	0.92	1.90	0.39	0.33	0.08	0.02	0.03	0.07	0.03	0.02
17469	0.92	1.88	0.51	0.44	0.10	0.02	0.01	0.02	0.01	0.01
19165	0.93	1.97	0.49	0.39	0.11	0.01	0.01	0.06	0.01	0.01
29796	0.93	1.90	0.51	0.46	0.10	0.01	0.01	0.05	0.02	0.01
30872	0.93	1.88	0.36	0.28	0.09	0.01	0.01	0.06	0.02	0.01
32940	0.92	1.87	0.48	0.48	0.09	0.01	0.01	0.09	0.01	0.01
Amytis	0.93	1.93	0.50	0.40	0.11	0.03	0.01	0.05	0.01	0.03
Feldberg1	0.93	1.91	0.38	0.32	0.09	0.02	0.01	0.09	0.01	0.01
Feldberg2	0.93	1.92	0.40	0.33	0.10	0.01	0.02	0.06	0.01	0.01
Incidentia1	0.94	2.00	0.46	0.35	0.11	0.01	0.01	0.07	0.01	0.01
Incidentia2	0.94	1.92	0.44	0.35	0.11	0.01	0.01	0.08	0.01	0.01
Jeanloup	0.93	1.89	0.49	0.37	0.10	0.01	0.02	0.04	0.01	0.01
Kanatsu	0.93	1.94	0.51	0.41	0.11	0.01	0.01	0.04	0.01	0.01
Kourakuen	0.93	1.90	0.40	0.34	0.09	0.02	0.01	0.08	0.02	0.01
Kuga	0.93	1.94	0.39	0.32	0.10	0.02	0.01	0.10	0.01	0.02
Rotaryusa	0.92	1.88	0.45	0.42	0.09	0.01	0.01	0.06	0.01	0.01
Ruff	0.93	1.91	0.48	0.38	0.10	0.01	0.03	0.04	0.02	0.01
Shiretoko	0.94	1.97	0.45	0.30	0.11	0.01	0.01	0.11	0.01	0.01
Stohl1	0.93	1.90	0.35	0.29	0.09	0.01	0.01	0.09	0.01	0.01
Stohl2	0.93	1.91	0.36	0.28	0.09	0.01	0.01	0.08	0.01	0.01
Swope1	0.93	1.90	0.43	0.36	0.09	0.01	0.03	0.08	0.02	0.01
Swope2	0.93	1.94	0.37	0.35	0.09	0.01	0.02	0.12	0.02	0.01
Swope3	0.93	1.90	0.43	0.36	0.09	0.02	0.02	0.09	0.03	0.02
Veteraniya	0.93	1.91	0.37	0.30	0.09	0.01	0.01	0.08	0.01	0.01

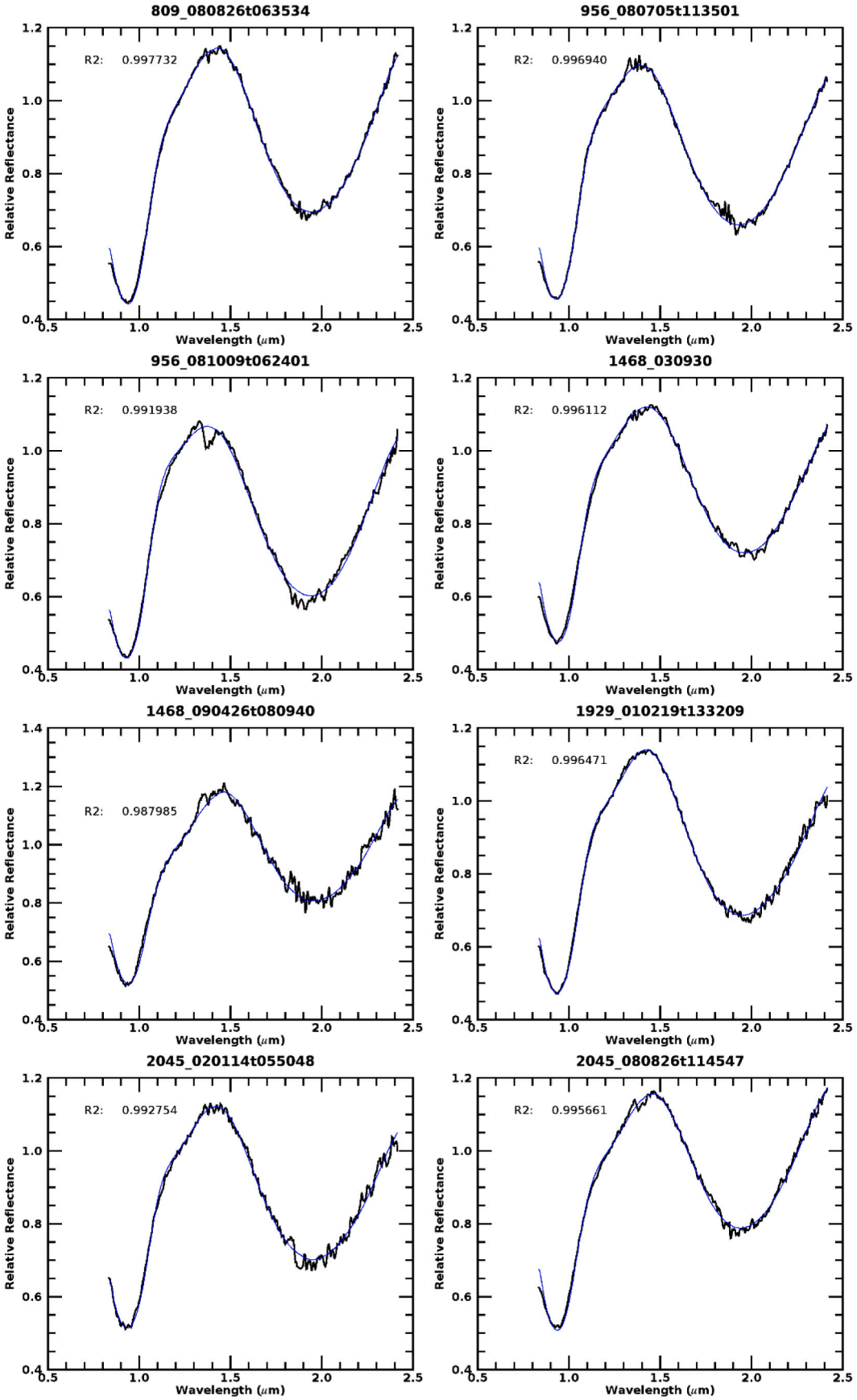

Fig. 1. Hapke model (blue line) on asteroids dataset (black line). (For interpretation of the references to colour in this figure legend, the reader is referred to the web version of this article.)

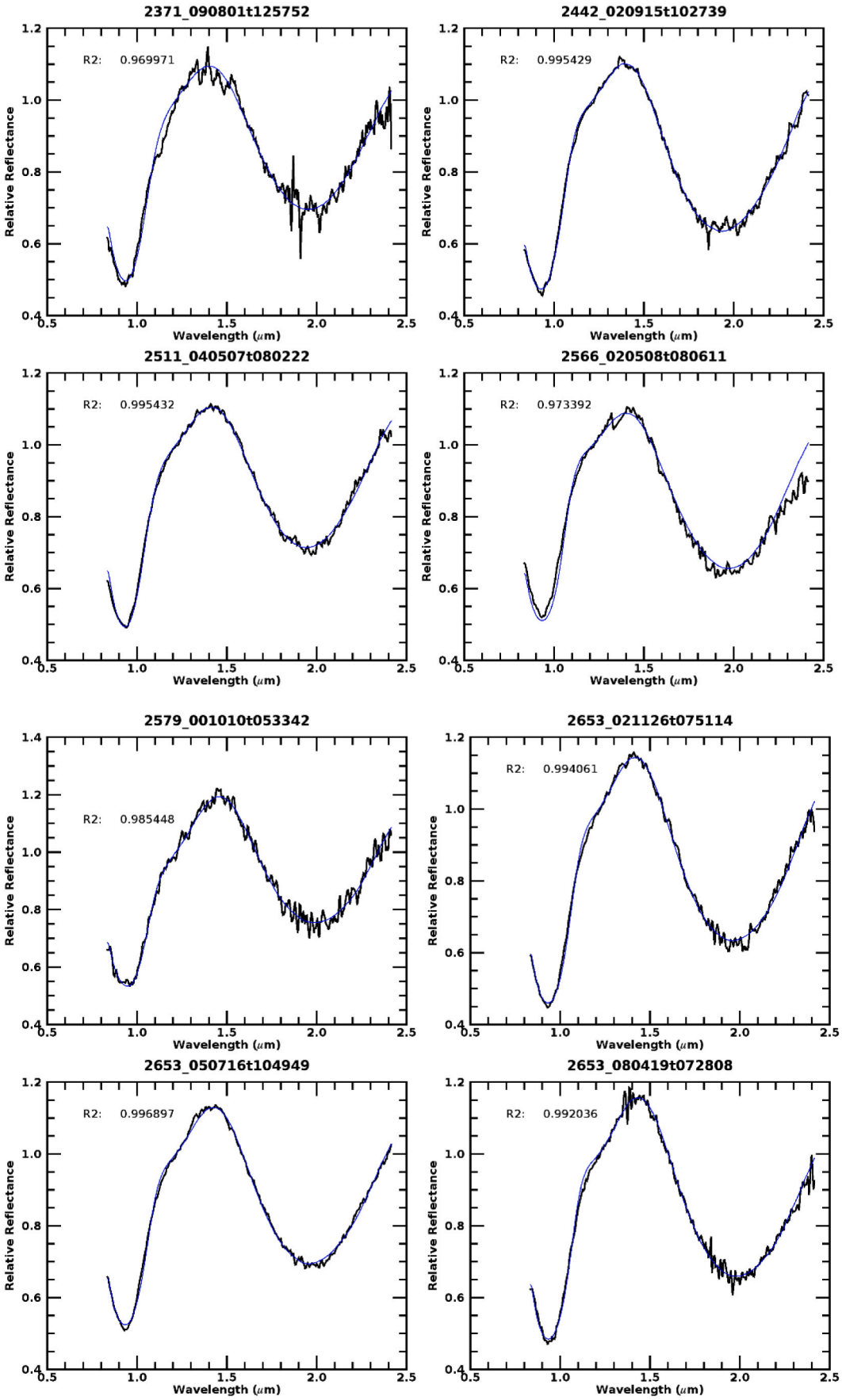

Fig. 1. (*continued*).

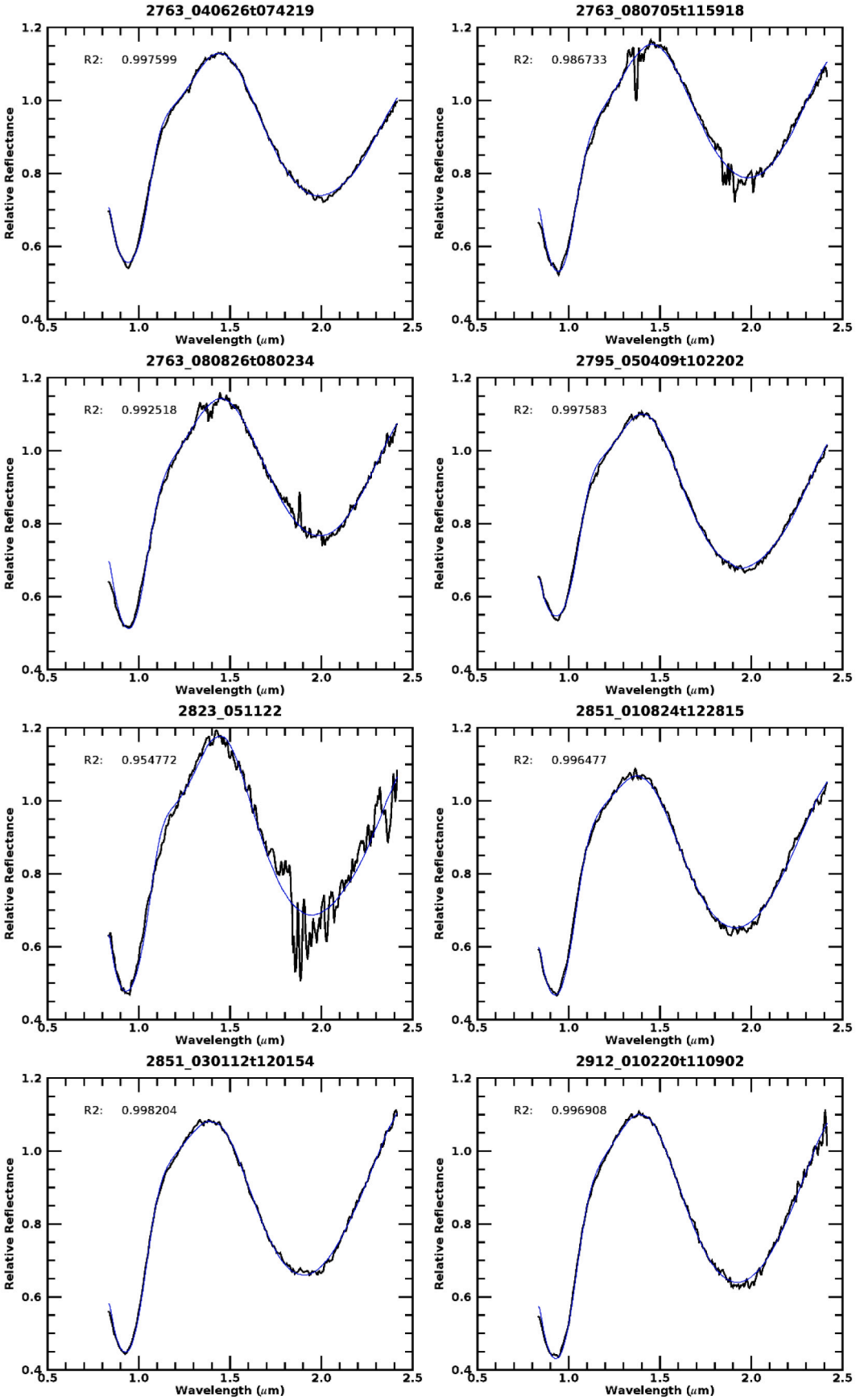

Fig. 1. (*continued*).

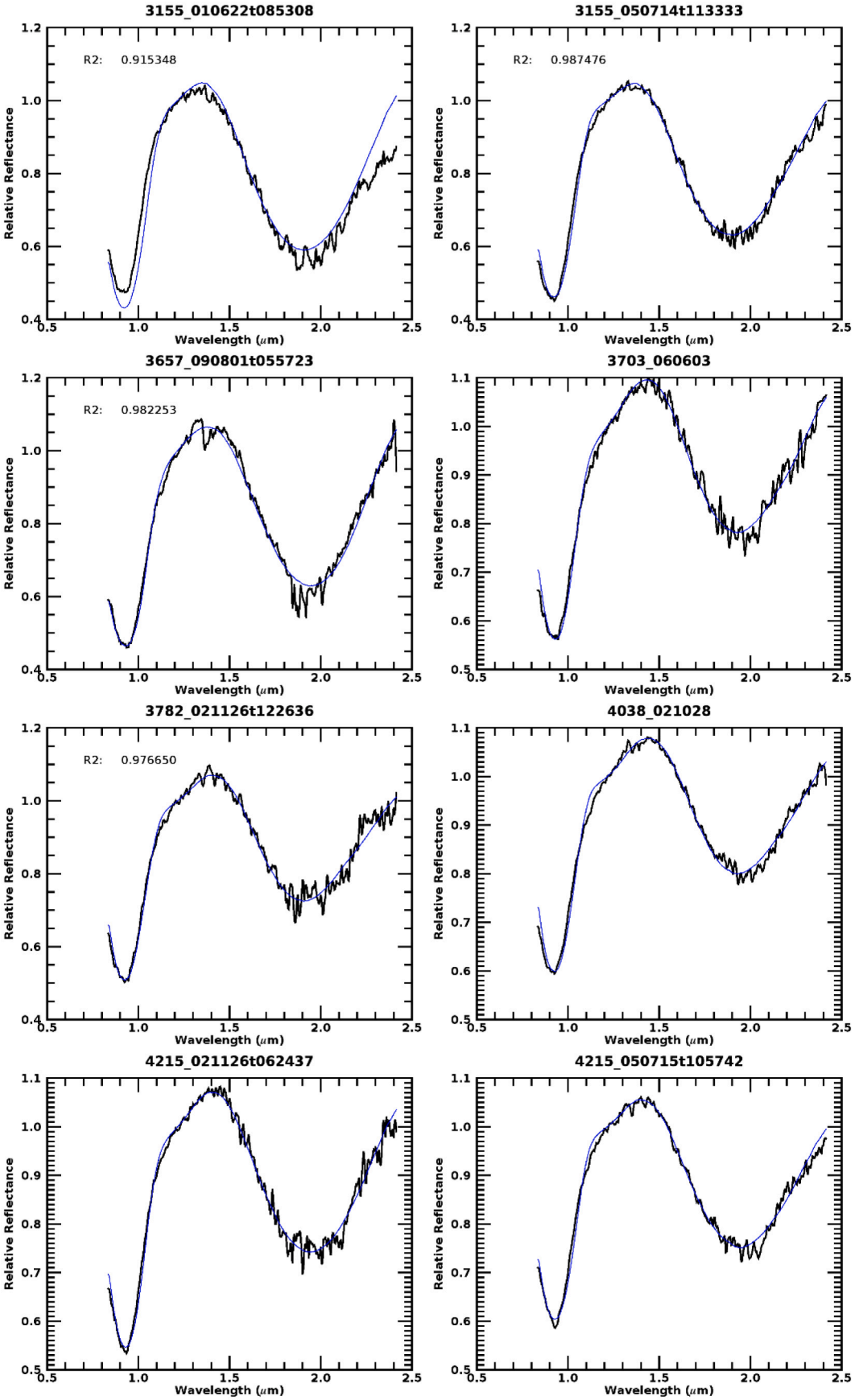

Fig. 1. (*continued*).

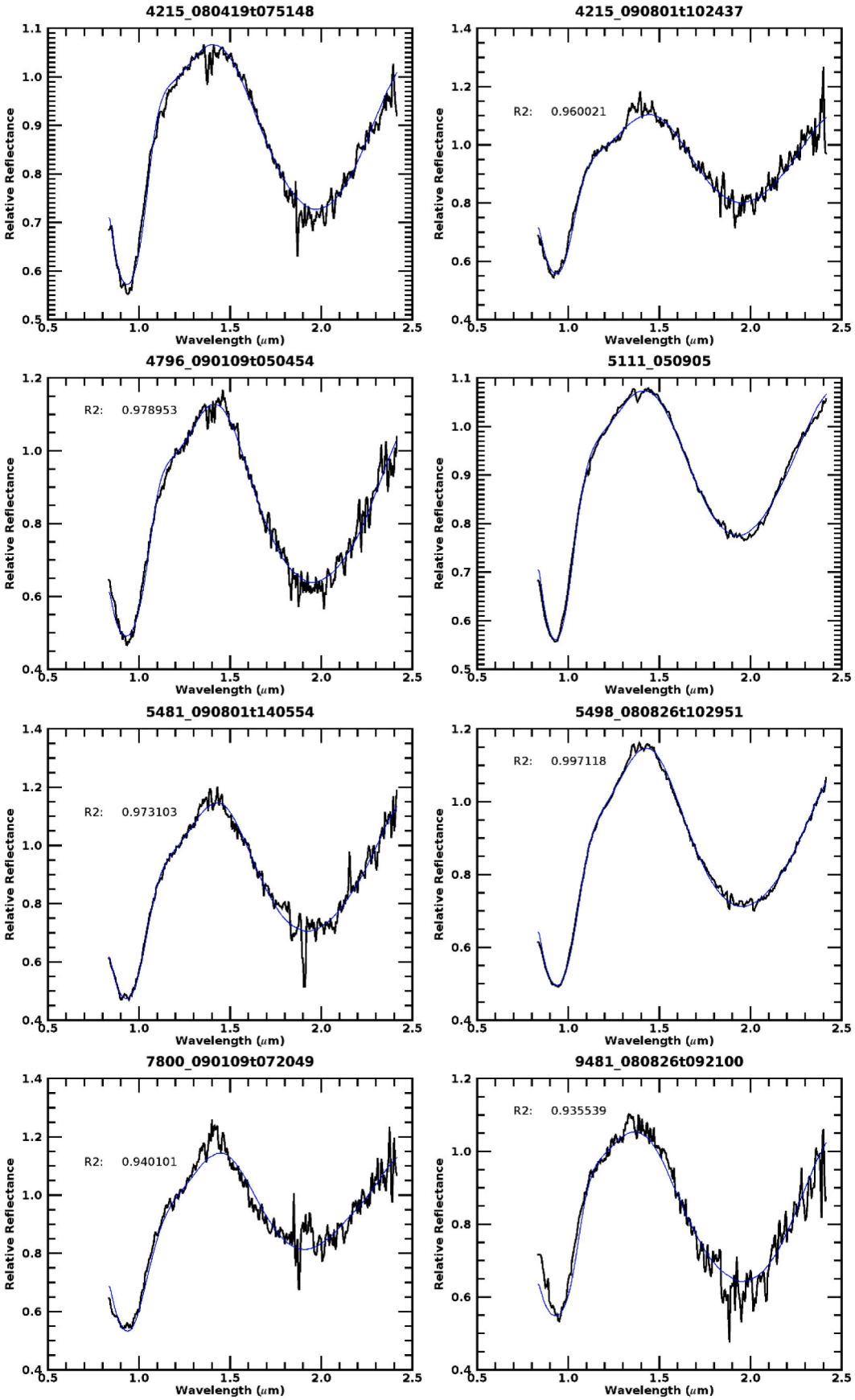

Fig. 1. (*continued*).

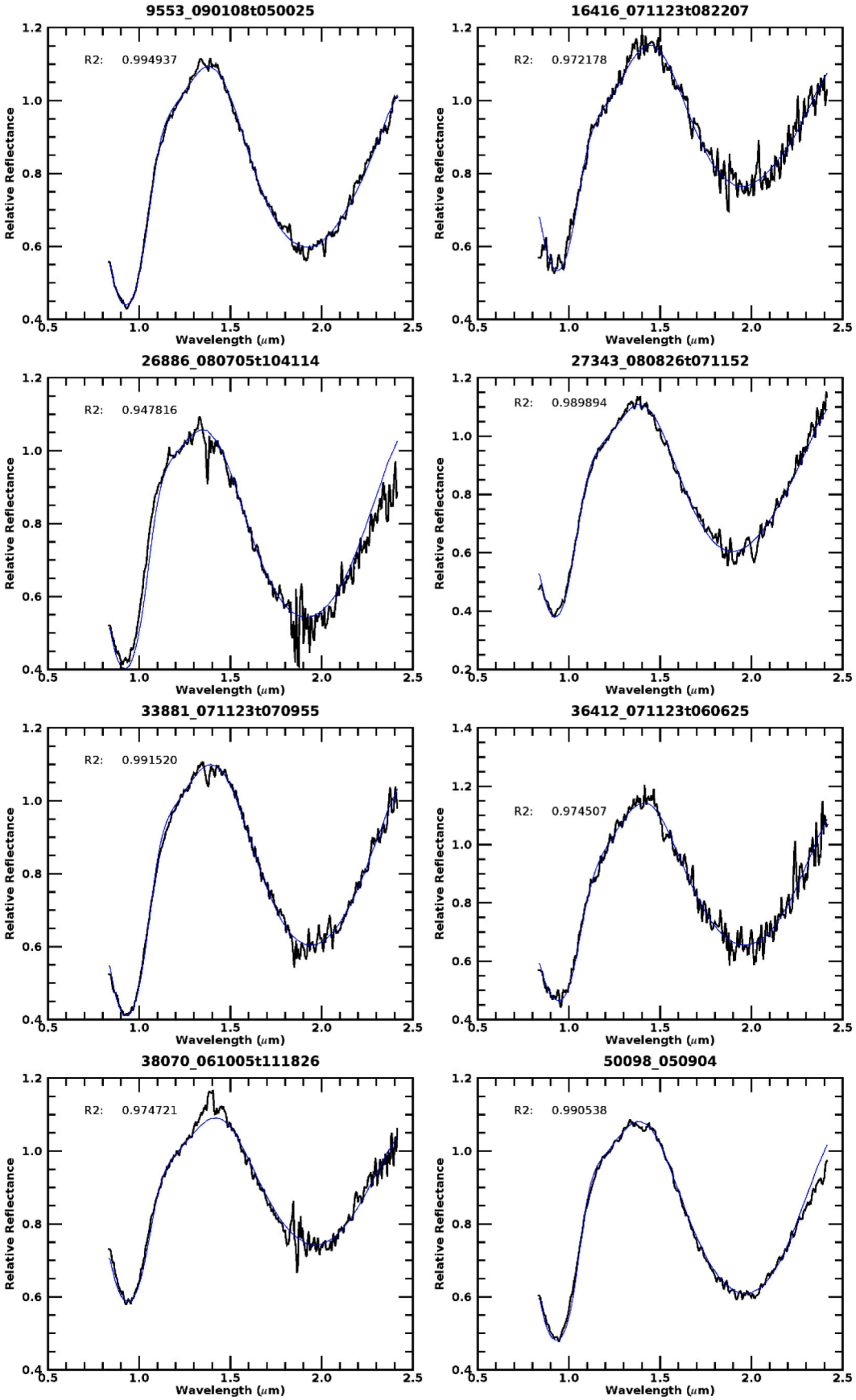

Fig. 1. (*continued*).

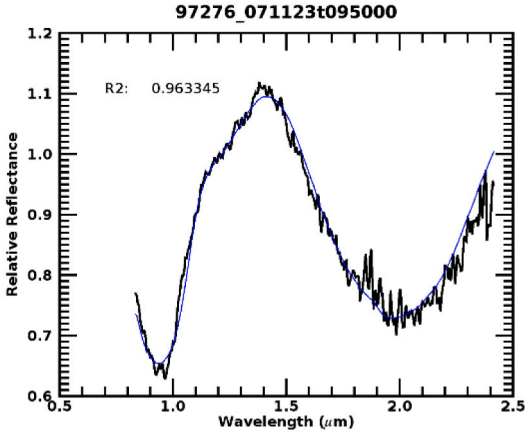

Fig. 1. (*continued*).

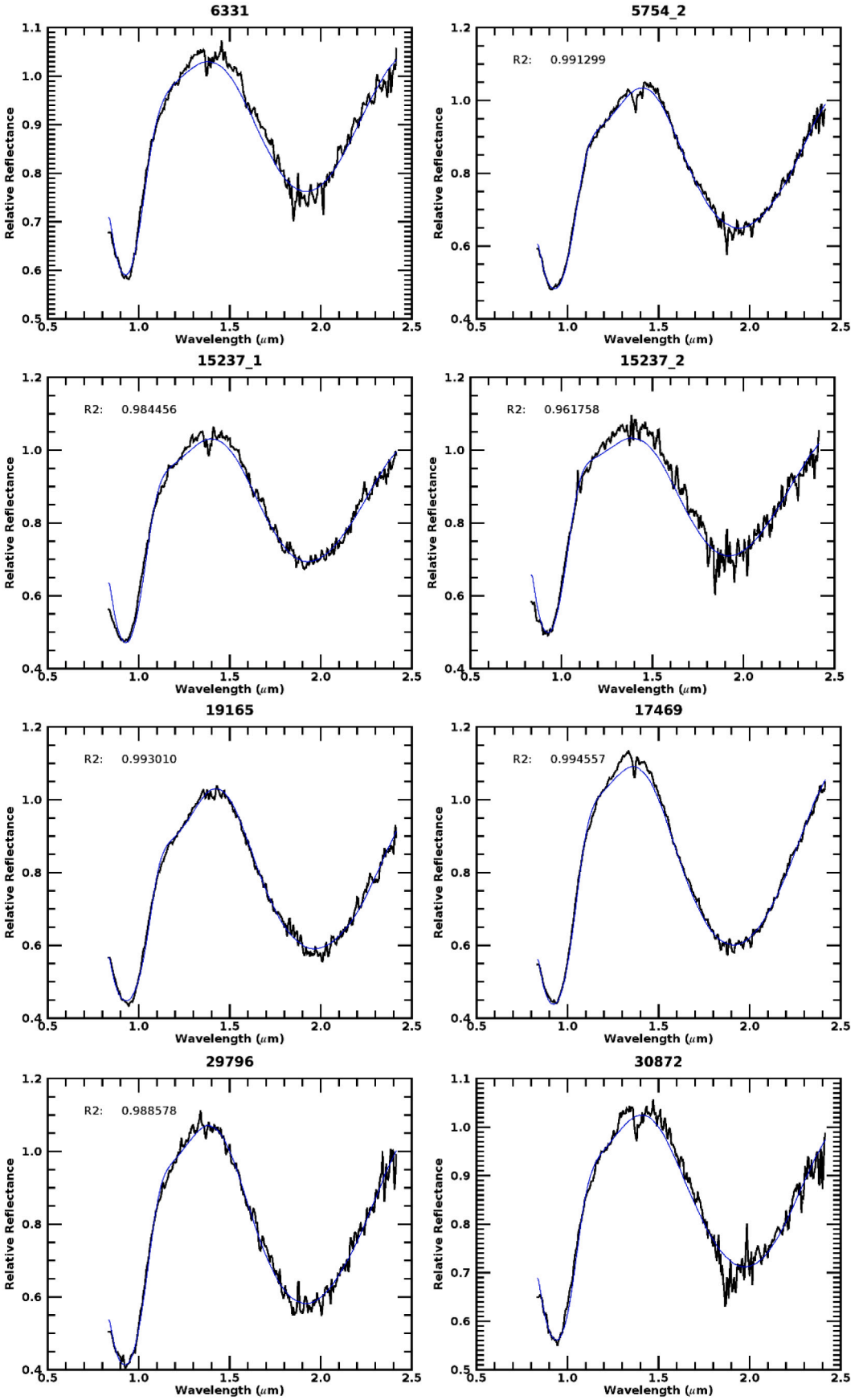

Fig. 2. Group 2 of V-type spectra (black line) and Hapke fit (blue line). (For interpretation of the references to colour in this figure legend, the reader is referred to the web version of this article.)

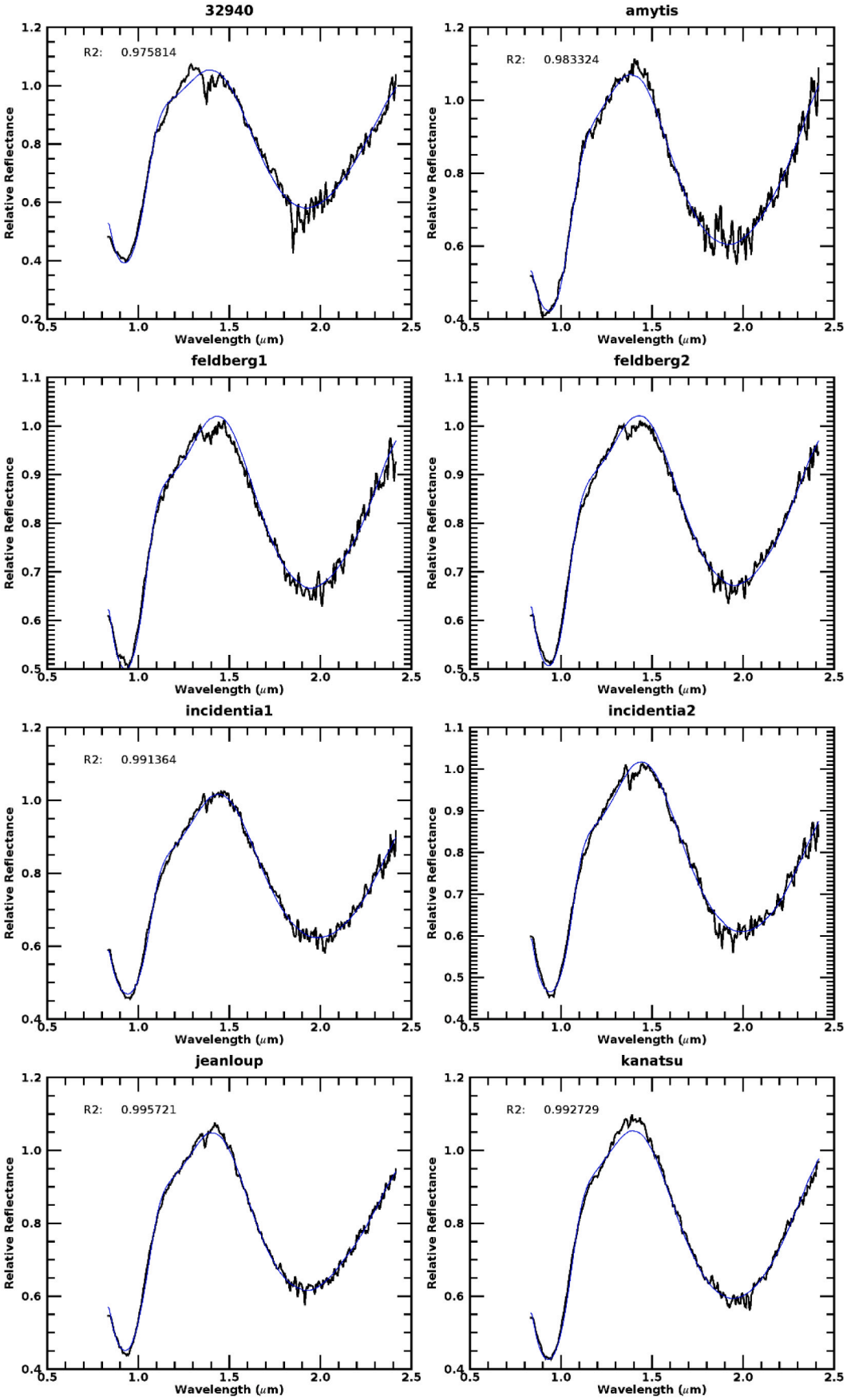

Fig. 2. (*continued*).

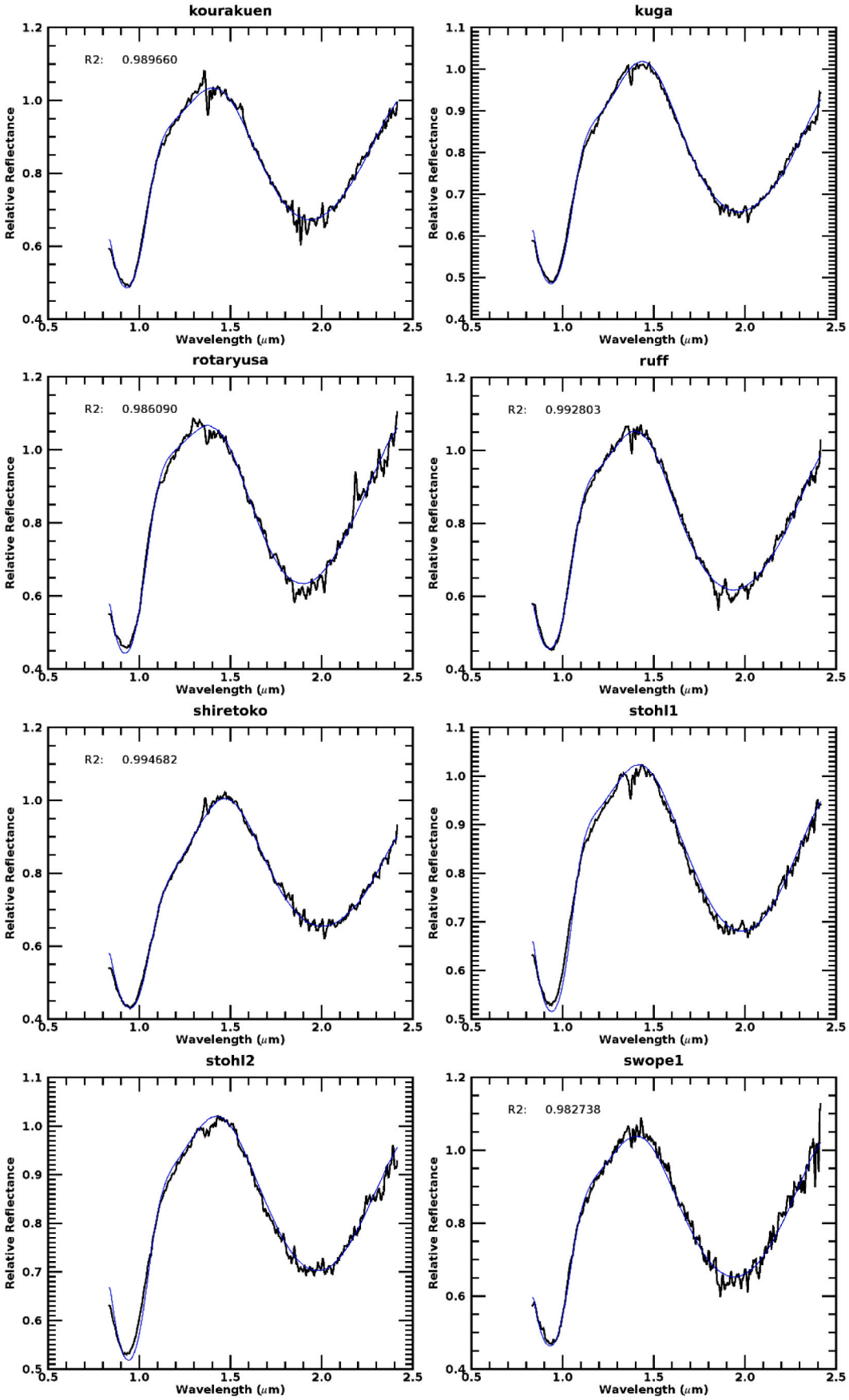

Fig. 2. (*continued*).

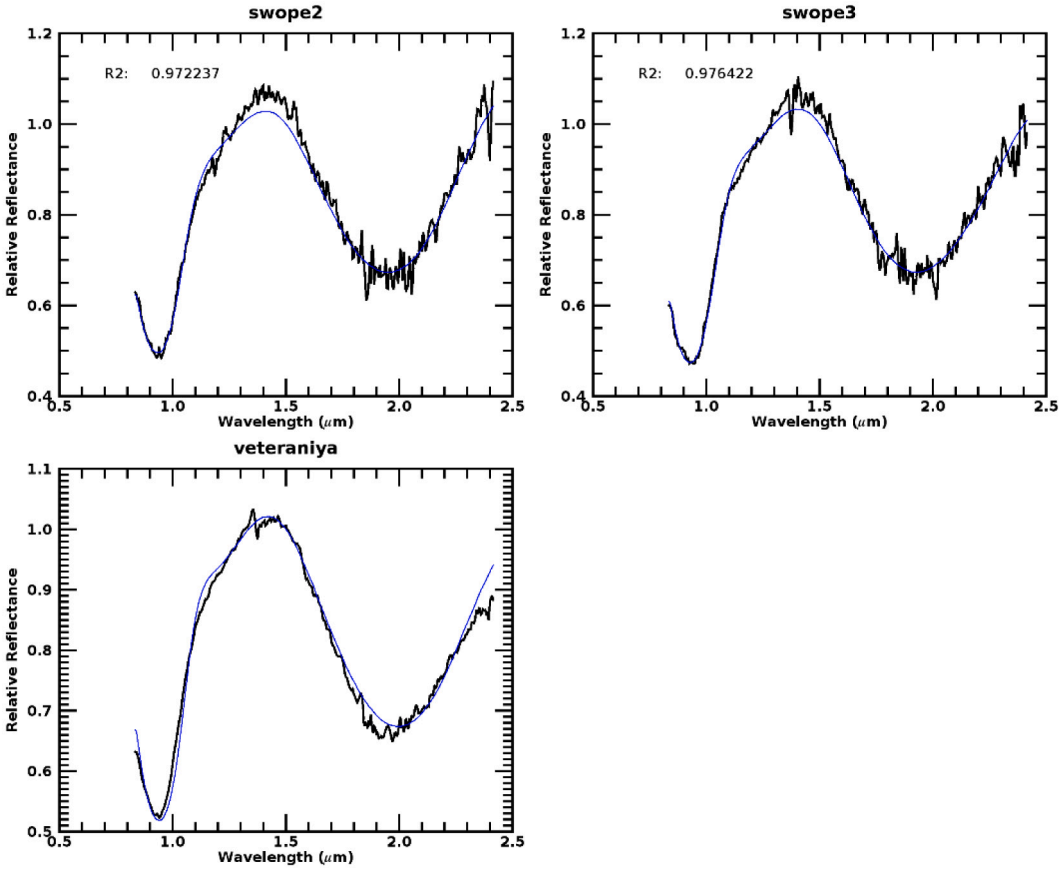

Fig. 2. (*continued*).

References

Ammannito, E., et al., 2013. Vestan lithologies mapped by the visual and infrared spectrometer. Meteorit. Planet. Sci. 48 (11), 2185–2198. https://doi.org/10.1111/maps.12192.

Barrat, J.A., et al., 2010. Relative chronology of crust formation on asteroid Vesta: Insights from the geochemistry of diogenites. Geochim. Cosmochim. Acta 74 (21), 6218–6231. https://doi.org/10.1016/j.gca.2010.07.028.

Birlan, M., et al., 2014. Spectroscopy and surface properties of (809) Lundia, 2014 MNRAS 437, 176–184. https://doi.org/10.1093/mnras/stt1869.

Burbine, T.H., et al., 2001. Vesta, Vestoids, and the howardite, eucrite, diogenite group: Relationships and the origin of spectral differences. Meteorit. Planet. Sci. 36, 761–781. https://doi.org/10.1111/j.1945-5100.2001.tb01915.x.

Burbine, T.H., et al., 2009. Pyroxene mineralogies of near-Earth vestoids. Meteorit. Planet. Sci. 44 (9), 1331–1341. https://doi.org/10.1111/j.1945-5100.2009.tb01225.x.

Capria, M.T., et al., 2014. Vesta surface thermal properties map. Geophys. Res. Lett. 41 (5), 1438–1443. https://doi.org/10.1002/2013GL059026.

Carruba, V., et al., 2007. Modeling close encounters with massive asteroids: a Markovian approach. A&A 465, 315–330. https://doi.org/10.1051/0004-6361:20066056.

Cloutis, E.R., Gaffey, M.J., 1991. Pyroxene spectroscopy revisited: spectral-composition-correlations and relationship to geothermometry. J. Geophys. Res. 96 (E5) https://doi.org/10.1029/91JE02512. PAGES 22,809-22,826.

Cloutis, E., et al., 1986. Calibrations of phase abundance, composition, and particle size distribution for olivine-orthopyroxene mixtures from reflectance spectra. J. Geophys. Res. 91 (B11) https://doi.org/10.1029/JB091iB11p11641, 11,641-11,653.

Cloutis, E., et al., 2013. Spectral reflectance properties of HED meteorites + CM2 carbonaceous chondrites: comparison to HED particle size and compositional variations and implications for the nature of low-albedo features on Asteroid 4 Vesta, 2013 Icarus 223, 850–877. https://doi.org/10.1016/j.icarus.2013.02.003.

De Sanctis, M.C., et al., 2011. Mineralogical characterization of some V-type asteroids, in support of the NASA Dawn mission. Mon. Not. R. Astron. Soc. 412, 2318–23332. https://doi.org/10.1111/j.1365-2966.2010.18058.x.

De Sanctis, M.C., et al., 2012. Spectroscopic characterization of mineralogy and its diversity across Vesta. SCIENCE 336. https://doi.org/10.1126/science.1219270.

De Sanctis, M.C., , et al.Meteorit., 2013. Vesta's mineralogical composition as revealed by the visible and infrared spectrometer on Dawn. Planet. Sci. 48 (11), 2166–2184. https://doi.org/10.1111/maps.12138.

DeMeo, F.E., et al., 2009. An extension of the Bus asteroid taxonomy into the near-infrared. Icarus 202, 160–180. https://doi.org/10.1016/j.icarus.2009.02.005.

Duffard, D., et al., 2004. Mineralogical characterization of some basaltic asteroids in the neighborhood of (4) Vesta: first results. Icarus 171,120–132. https://doi.org/10.1016/j.icarus.2004.05.004.

Duffard, D., Roig, F., 2009. Two new V-type asteroids in the outer Main Belt? Icarus 57 (2).

Galiano, A., et al., 2018. Continuum definition for 3.1, 3.4 and 4.0 μm absorption bands in Ceres spectra and evaluation of effects of smoothing procedure in the retrieved spectral parameters. Adv. Space Res. 62, 2342–2354. https://doi.org/10.1016/j.asr.2017.10.039.

Gundlach, B., Blum, J., 2013. A new method to determine the particle size of planetary regolith. Icarus 223, 479–492. https://doi.org/10.1016/j.icarus.2012.11.039.

Hammergren, M., et al., 2006. arXiv, (21238)1995 WV7: A new basaltic asteroid outside the 3:1Mean Motion Resonance arXiv:astro-ph/0609420.

Hapke, B., et al., 1981. Bidirectional reflectance spectroscopy 1. Theory. J. Geophys. Res. 86 (B4), 3039–3054. https://doi.org/10.1029/JB086iB04p03039.

Hapke, B., et al., 2012. Theory of Reflectance and Emittance Spectroscopy. Cambridge University Press.

Hardersen, P.S., et al., 2014. More chips off of Asteroid (4) Vesta: Characterization of eight Vestoids and their HED meteorite analogs. Icarus 242, 269–282. https://doi.org/10.1016/j.icarus.2014.08.020.

Hardersen, P.S., et al., 2015. Vestoids, Part II: The basaltic nature and hed meteorite analogs for eight Vp-Type asteroids and their associations with (4) Vesta. Astrophys. J. Suppl. Ser. 221, 19. https://doi.org/10.1088/0067-0049/221/1/19.

Hardersen, P.S., et al., 2018. Basalt or not? near-infrared spectra, surface mineralogical estimates, and Meteorite Analogs for 33 Vp-type asteroids. Astron. J. 156, 11. https://doi.org/10.3847/1538-3881/aac3d2.

Hiroi, T., et al., 1995. Particle size and mineral compositions of surface regoliths of Vesta-like asteroids. Icarus 374–386. https://doi.org/10.1006/icar.1995.1105.

Ieva, S., et al., 2016. Spectral characterization of V-type asteroids – II. A statistical analysis. MNRAS 455, 2871–2888. https://doi.org/10.1093/mnras/stv2510.

Jaumann, R., et al., 2014. The geological nature of dark material on Vesta and implications for the subsurface structure. Icarus 240, 3–19. https://doi.org/10.1016/j.icarus.2014.04.035.

Klima, Rachel L., Pieters, Carlé M., Dyar, M. Darby, 2008. Characterization of the 1.2 μm M1 pyroxene band: Extracting cooling history from near-IR spectra of pyroxenes and pyroxene-dominated rocks. Meteoritics & Planetary Science 10, 1591–1604.

Lazzaro, D., et al., 2000. Discovery of basaltic asteroid in the outer main belt. Science 288 (5473), 2033–2035. https://doi.org/10.1126/science.288.5473.2033.

Le Corre, et al., 2015. Exploring exogenic sources for the olivine on Asteroid (4) Vesta. Icarus 258, 483–499.
Lim, L.F., et al., 2011. Mineralogy and thermal properties of V-type Asteroid 956 Elisa: evidence for diogenitic material from the Spitzer IRS (5–35 μm) spectrum. Icarus 213, 510–523. https://doi.org/10.1016/j.icarus.2010.12.006.
Longobardo, A., et al., 2014. Photometric behavior of spectral parameters in Vesta dark and bright regions as inferred by the Dawn VIR spectrometer. Icarus 240, 20–35. https://doi.org/10.1016/j.icarus.2014.02.014.
Lucey, Paul G., 1998. Model near-infrared optical constants of olivine and pyroxene as a function of iron content. J. Geophys. Res. 103, 1703–1713.
Marchi, S., et al., 2012. The violent collisional history of asteroid 4 Vesta. SCIENCE 336 (6082), 690–694. https://doi.org/10.1126/science.1218757.
McCord, et al., 1970. Asteroid Vesta: spectral reflectivity and compositional implications. Science 1445–1447. https://doi.org/10.1126/science.168.3938.1445.
McCord, et al., 2012. Dark material on Vesta from the infall of carbonaceous volatile-rich material. Nature 491, 83–86. https://doi.org/10.1038/nature11561.
McSween, H.Y.J., et al., 2011. HED meteorites and their relationship to the geology of Vesta and the Dawn mission. Space Sci. Rev. 141–174. https://doi.org/10.1007/978-1-4614-4903-4_9.
McSween, H.Y.J., et al., 2013. Dawn; the Vesta–HED connection; and the geologic context for eucrites, diogenites, and howardites. Meteorit. Planet. Sci. 48 (11), 2090–2104. https://doi.org/10.1111/maps.12108.
Mittlefehldt, D.W., et al., 2015. Asteroid (4) Vesta: I. The howardite-eucrite-diogenite (HED) clan of meteorites. Chem. Erde 75, 155–183. https://doi.org/10.1016/j.chemer.2014.08.002.
Moskovitz, N.A., et al., 2008. The distribution of basaltic asteroids in the Main Belt. Icarus 198 (1), 77–90. https://doi.org/10.1016/j.icarus.2008.07.006.
Moskovitz, N.A., et al., 2010. A spectroscopic comparison of HED meteorites and V-type asteroids in the inner Main Belt. Icarus 208, 773–788. https://doi.org/10.1016/j.icarus.2010.03.002.
Nesvorny, D., et al., 2008. Icarus. Fugitives from the Vesta family 183, 85–95. https://doi.org/10.1016/j.icarus.2007.08.034.
Palomba, E., et al., 2014. Composition and mineralogy of dark material units on Vesta. Icarus 240, 58–72. https://doi.org/10.1016/j.icarus.2014.04.040.
Palomba, E., et al., 2015. Detection of new olivine-rich locations on Vesta. Icarus 258, 120–134. https://doi.org/10.1016/j.icarus.2015.06.011.
Palomba, E., et al., 2019. Detection of crystalline and fine-grained calcic plagioclases on vesta. Astrophys. J. Lett. 882, L22, 7pp. https://doi.org/10.3847/2041-8213/ab339e.
Roig, F., et al., 2008. V-type asteroids in the middle main belt. Icarus 194 (1), 125–136. https://doi.org/10.1016/j.icarus.2007.10.004.
Roush, T.L., et al., 2005. Near-infrared (0.67–4.7 μm) optical constants estimated. Icarus 179, 259–264. https://doi.org/10.1016/j.icarus.2005.06.004.
Ruesch, O., et al., 2014. Detections and geologic context of local enrichments in olivine on Vesta with VIR/Dawn data. J. Geophys. Res. 119 (9), 2078–2108. https://doi.org/10.1002/2014JE004625.
Shearer, C.K., Burger, P., Papike, J.J., 2010. Petrogenetic relationships between diogenites and olivine diogenites: Implications for magmatism on the HED parent body. Geochimica et Cosmochimica Acta 74, 4865–4880.
Turrini, D., et al., 2016. Olivine on Vesta as exogenous contaminants brought by impacts: constraints from modeling Vesta's collisional history and from impact simulations. Icarus 280, 328–339. https://doi.org/10.1016/j.icarus.2016.07.009.
Williams, D.A., et al., 2014. The chronostratigraphy of protoplanet Vesta. Icarus 244, 158–165. https://doi.org/10.1016/j.icarus.2014.06.027.
Yamaguchi, A., Mikouchi, T., Shirai, N., Ebihara, M., Barrat, J.A., Messenger, S, 2011. Heating Experiments of a Basaltic Eucrite and Implications for Chronology and Geochemistry. Workshop Formation First Solids Solar Syst. Contribution No. 1639.